The performance analysis of a new thermal backfill material for underground power cable system

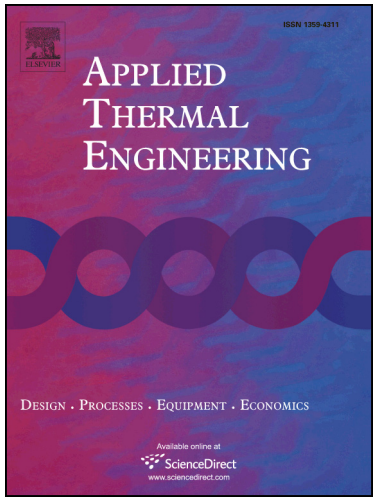

The performance analysis of a new thermal backfill material for underground power cable system

Paweł Ocłoń, Marco Bittelli, Piotr Cisek, Eva Kroener, Marcin Pilarczyk, Dawid Taler, Ravipudi Venkata Rao, Andrea Vallati

PII: S1359-4311(16)31233-9
DOI: http://dx.doi.org/10.1016/j.applthermaleng.2016.07.102
Reference: ATE 8700

To appear in: *Applied Thermal Engineering*

Received Date: 29 February 2016
Revised Date: 13 June 2016
Accepted Date: 15 July 2016

Please cite this article as: P. Ocłoń, M. Bittelli, P. Cisek, E. Kroener, M. Pilarczyk, D. Taler, R.V. Rao, A. Vallati, The performance analysis of a new thermal backfill material for underground power cable system, *Applied Thermal Engineering* (2016), doi: http://dx.doi.org/10.1016/j.applthermaleng.2016.07.102

The performance analysis of a new thermal backfill material for underground power cable system

Paweł Ocłoń[a,*], Marco Bittelli[b], Piotr Cisek[a], Eva Kroener[c], Marcin Pilarczyk[a], Dawid Taler[d], Ravipudi Venkata Rao[e], Andrea Vallati[f]

[a] *Institute of Thermal Power Engineering, Cracow University of Technology, al. Jana Pawła II 37, 31-864 Kraków, Poland*

[b] *Department of Agricultural Sciences, University of Bologna, VialeFanin 44, 40125 Bologna, Italy*

[c] *Division of Soil Hydrology, Georg August University of Göttingen, Büsgenweg 2, 37077 Göttingen, Germany*

[d] *Institute of Thermal Engineering and Air Protection, Cracow University of Technology, ul. Warszawska 24, 31-155 Kraków, Poland*

[e] *SardarVallabhbhai National Institute of Technology (SV NIT) Ichchanath, Surat-395 007, Gujarat State, India*

[f] *Dept. of Astronautical, Electrical and Energetic Engineering, Sapienza University of Rome, Via Eudossiana, 18 00184 Rome, Italy*

[*] *Corresponding author. E-mail address:* poclon@mech.pk.edu.pl (P.Ocłoń)

Abstract: Lafarge Gruntar™ material is proposed in this paper as a new thermal backfill component, and different mass fractions such as 5%, 10%, and 15% are examined. The thermal properties of the developed backfill are determined by experiments with respect to water content and time. Based on the experimental data it is found that the 15% mass fraction Lafarge Gruntar*TM* material provides the most favorable thermal conductivity i.e. over 1.00 W/(m K) in the dry state. This paper also presents a thermal performance optimization procedure for the high voltage underground power cable system. The new thermal backfill material is considered to be installed within the cable system to improve its thermal performance. The analyzed system consists of three underground power cables situated in a flat formation (in−line arrangement) in thermal backfill, buried in the native soil. To avoid extensive mechanical loads caused by vibrations, when locating beneath a paved ground (e.g. under road crossings), the cables are situated in High Density Polyethylene (HDPE) casing pipes filled with sand−bentonite mixture. The pipes are then placed into a thermal backfill and buried in the native soil. The Installation of thermal backfill material is relatively expensive since in many cases the buried line is installed over many kilometers. Therefore, it is important to determine the optimal dimensions of the cable bedding layer to minimize the material and installation costs while keeping efficient heat dissipation from the cables. The momentum-type Particle Swarm Optimization (PSO) solver, with a dynamic penalty function, is used to minimize the cable backfill cross-sectional area while not exceeding the allowable temperature of the cable operation. The performed optimization procedure obtains the converged solution. The temperature distribution in soil, cables, and the cable backfill layer is

determined using the Finite Element Method. The Campbell − de Vries thermal conductivity model is employed for the soil surrounding the underground power cable system. An MATLAB code is written for solving the heat conduction equation and to determine the temperature distribution within the underground power cable system. By using the momentum-type Particle Swarm Optimization algorithm, it is possible to design the best-found dimensions of the cable bedding layer (width and height). Moreover, the dynamic penalty function employed in the optimization procedure has assured the determination of the maximum temperature of cable conductor close to its best-found value.

Keywords: momentum-type particle swarm optimization, underground power cables, thermal conductivity, heat dissipation, thermal backfill

Nomenclature

A	cross-section area,m^2
b	distance between conductor axis and top edge of the FTB bedding layer, m
d	diameter, m
D_v	vapour diffusivity, m^2/s
e_a	partial vapour pressure, Pa
f	alternating current (AC) frequency, Hz
$F(\boldsymbol{x})$	cost function,
$f(\boldsymbol{x})$	original objective function,
g	shape factor, -
$g_j(\boldsymbol{x})$	inequality constrained function,
$gbest$	global best position,
H	cable line burial depth, m
$h_j(\boldsymbol{x})$	equality constrained function,
I	current load, A
k	weighting factor in Campbell-De Vries model, -
k_s	skin effect correction factor, -
k_p	proximity effect correction factor, -
L_v	latent heat of vaporization, kJ/kg
l	distance between conductor axes, m

Greek Symbols

α	parameter of momentum-type PSO algorithm,
$\alpha_{e,ref}$	temperature coefficient for the conductor material, -
β	parameter of momentum-type PSO algorithm,
δ	thickness, mm
ε	convergence criterion,
ΔQ	heat losses from the power cable per unit length, W/km
θ	volumetric fraction of water,
λ	thermal conductivity, W/(mK)]
ρ	molar density of air, m^3/kmol
ϕ	volumetric fraction,

Subscripts

a	air,
AC	alternating current,
b	backfill,
c	cable conductor,
DC	direct current,
e	external,
$final$	final,

m_y	fractional clay content, -
N_{par}	number of particles in a swarm, -
P	atmospheric pressure, Pa
p	distance between conductor axis and bottom edge of the FTB bedding layer, m
pbest	best particle position,
q_v	heat source per unit volume, W/m^3
r	Radius, m
R_e	electric resistance, Ω/km
s	distance between conductor axis and lateral edge of the FTB bedding layer, m
T	temperature, °C
$T_{c\,\max}$	central cable core maximum temperature, °C
$T_{c,FEM}$	cable core temperature determined from FEM model, °C
$\boldsymbol{v}_i^n$	velocity of *i*-th particle in *n*-th iteration,
w	gravimetric water content, %
$\mathbf{x}$	vector of design variables,
x	horizontal cartesiancoordinate,
x_s	proximity effect factor, -
$\boldsymbol{x}_i^n$	position of the *i*-th particles in *n*-th iteration,
y	vertical cartesiancoordinate,
y_s	skin effect factor, -
y_p	proximity effect factor, -

g	gas,
init	initial,
ins	cable insulation,
int	internal,
ja	cable jacket,
max	maximum value ,
mean	mean value,
min	minimum value,
opt	optimal value ,
s	solid,
surf	at ground level,
sh	cable sheath,
out	outer,
ref	reference value,
w	water,

Superscripts

n	iteration number,
0	initial iteration,

1. Introduction

Underground cable lines installation has a long history dating back to 1890, when in the United Kingdom, the first successful installation was pioneered by Dr. Ferranti using HV (High Voltage) insulated conductors [1]. Over the past 100 years, significant progress in the development of high voltage cables construction has been made. One of the most valuable products developed for underground power cables was fluid-impregnated-paper-insulated cable, perfected by Emanuelli from Pirelli Company. The next milestone was the application of cross-linked polyethylene (XLPE) insulation, developed by General Electric in 1963 [1]. Currently, XLPE cable is adopted in most cases, owing to its characteristics of easy maintenance and low transmission losses.

The electrical performance of XLPE cable has significantly improved due to the advances in contaminant removal techniques from insulating materials [2]. Improved dielectric materials allow for a cost-effective production and greater reliability of power cable systems. Thus, the use of underground power cables in distribution and transmission networks has significantly increased in recent years. Due to the increase in demand for electric energy and growing population density in different regions, the application of power cables is growing rapidly [3]. Power cables are widely used in urban distribution networks owing to their ease of construction, and no interference with city appearance during installation when compared to overhead transmission lines [4]. In addition, cable lines are resistant to weather conditions and significantly reduce electromagnetic field emissions. Underground power cables are more reliable than overhead transmission lines when it comes to the cable line failure likelihood. On the other hand, underground cable line malfunctions are harder to detect. Moreover, maintenance and repair of the cable line are time-consuming and more expensive, compared with overhead lines. The underground cables themselves also have a higher unit price due to their construction complexity and greater production costs [3].

Replacing overhead bare conductors by underground cables is one of the solutions that can be used for reliability enhancement of the electric power distribution systems [3]. Many countries build up the electric grid based on underground cable lines. Denmark, for instance, plans to underground 75% of its electricity grid in the future. Almost 10% of the planned underground power lines are 400kV transmission lines [5]. Countries, such as Poland, use the underground power cables as a power output line of the new power units. In addition, the upgrading of the main electricity grid points often uses HV cable lines.

Increasing requirements regarding the power supply and underground cable lines are the challenges in optimizing the design of reliable power systems. The optimization procedure shall result in the proper design of power cable systems while providing the favorable heat exchange conditions. Moreover, enhanced heat dissipation conditions may lead directly to reduce conductor cross-section area, thereby allowing for reducing cable line installation costs without changes in transferring current loading.

Several attempts to optimize power cable systems have been made so far. Del Valle et al. [6] presented a detailed overview of the fundamental concepts of Particle Swarm Optimization (PSO) and its variants and provided a comprehensive survey of the power system applications. This analysis shows the potential of PSO in the optimization of Underground Power Cable System (UPCS).

Kovac et al. [7] proposed a numerical-stochastic technique developed for UPCS design. The presented method involved non-linear coupled electric-thermal modeling of underground cables and a stochastic optimization method using differential evolution. Al-Saud at al. [8] presented an optimization model for underground power cable thermal circuit based on generated gradient approach. The authors had demonstrated the use of nonlinear optimization in conjunction with finite element thermal field analysis. The sensitivities of the cable temperatures with respect to fluctuations in the cable circuit parameters were also included. Calculations were carried out to obtain an optimal design of selected cable thermal

parameters.

Moutassem and Anders [9] presented a method for configuring the locations of any number of underground cables to achieve the highest total ampacity. The optimal configuration was determined through a two-level optimization algorithm. At the outer level, a combinatorial optimization based on a genetic algorithm explored the different possible configurations, which were then evaluated according to its total ampacity by using a convex optimization algorithm. The convex optimization algorithm that formed the inner level of the optimization procedure was based on the barrier method.

Zarchi et al. [10] proposed a method to find the optimal configuration of the cables in a duct bank taking into account the current harmonics and their effects on the sheath losses. The optimal placement of cables that maximizes the total ampacity was found using PSO and Shuffled Frog Leaping Algorithm. Del-Pino-López [11] proposed a shielding cost optimization process combining finite element models and genetic algorithm. The dimensions and location of the most cost-effective shield that limits the magnetic field in a particular area, without restricting the current−carrying capacity of the mitigated cable were obtained. In addition, the effects of different materials, phase configurations, shield geometry and losses were analyzed.

In the above-mentioned papers, the complex thermo-electrical analysis was performed. Nevertheless, the soil thermal conductivity was considered as constant. This paper presents a different approach by incorporating a comprehensive soil thermal conductivity model. Indeed, the novel contribution of this paper is related to the application of a comprehensive numerical model for heat transfer in UPCS. The model includes the soil thermal conductivity based on the Campbell − de Vries approach. Most heat transfer models, solving the second Fourier's law for heat conduction, do not include the temperature dependence of thermal conductivity which is usually assumed to be independent of temperature. One of the novel approaches of this research is to include a model (based on previously published experimental evidence) that accounts for the variation of thermal conductivity with temperature, as described in Campbell et al. [12].

The proposed UPCS model is used for optimizing the cable backfill layer dimensions. The goal of the optimization is to reduce the size of the backfill layer and, consequently, the material costs, which are significant (about $130 per cubic meter). The momentum type Particle Swarm Optimization method is employed for this purpose. Moreover, the new thermal backfill material, based on the Lafarge company product, Gruntar™, is developed. Thermal conductivity measurements of the proposed backfill are carried out on the laboratory scale. The performed measurements have proved that the thermal conductivity of the proposed backfill in the dry state is approximately five times larger than in the dry soil. Thermal properties of the proposed mortar are comparable to the widely used FTB (Fluidized Thermal Backfill) mortar, but it is significantly cheaper (~$130 per cubic meter of FTB vs. ~$20 per cubic meter of novel mortar –when including only the material costs). Experimental analysis is carried out using Decagon Devices KD2 PRO equipment. During the experiments, the relationship between the

water content of the proposed mortar and its thermal conductivity is determined at different periods of time.

The computations, shown in this paper, consider the temperature dependent cable ampacity and thermal properties of ground and cable backfill mortar. Thus, the heat conduction problem may be regarded as non−linear. The momentum−type PSO optimization solver with dynamic penalty function is used to minimize the cable backfill cross−sectional area while not exceeding the allowable temperature of cable operation. The performed optimization procedure has obtained the converged solution after a relatively small number of iterations. The temperature distribution in soil, cable, and the cable backfill layer is determined using the Finite Element Method. The MATLAB code is developed for this purpose. The two-dimensional heat conduction problem is solved for nodal temperatures.

2. Cable line layout

In this paper, a system of three HV (400kV) XLPE cables, buried in the ground in the flat (in-line) arrangement is analyzed. The considered cables consist of a cable solid core, cross−linked polyethylene (XLPE) insulation, metallic sheath, and non-metallic outer covering. Additionally, each cable layer is separated by an insulating tape. The copper cable conductor is additionally segmented to reduce the current losses [13]. The layout and arrangement of the cable layers in the considered power cable are shown in Fig. 1.

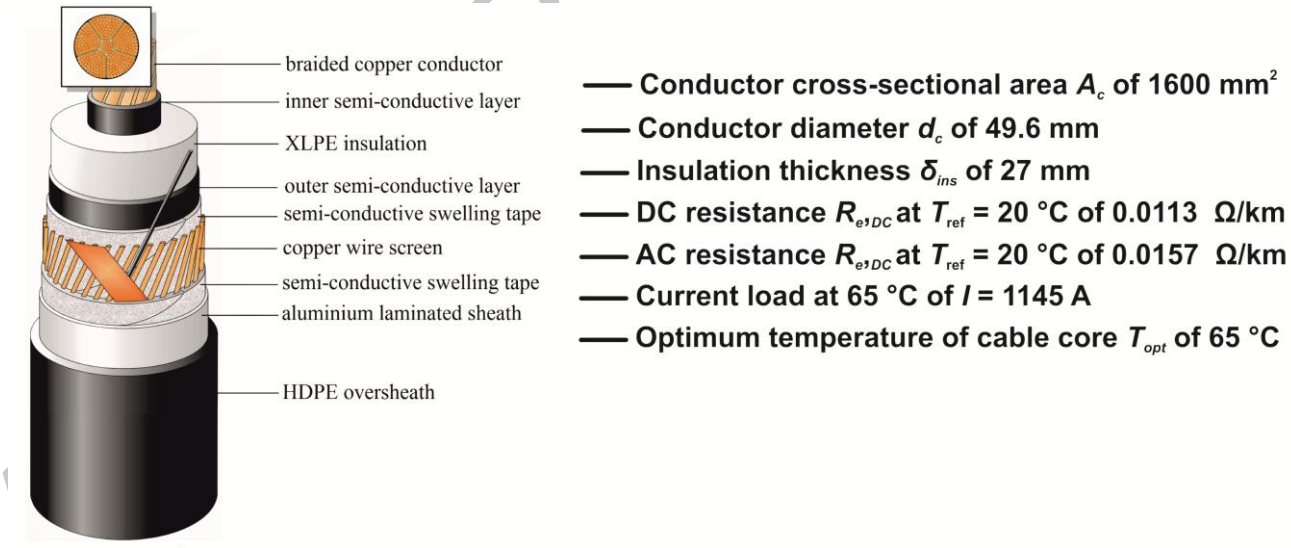

Fig. 1 The High Voltage cable design [13]

The most vulnerable to overheating part of the cable line are the places where underground power cables are installed in conduits. That burial technique is widely applied when the ground is subjected to unusually heavy loads (i.e. significant vibrations), i.e. under road and railway crossings. In that case, PVC (polyvinyl chloride) or PE (polyethylene) casing pipes are filled with sand-bentonite mixture (SBM). SBM improves the heat dissipation process from hot cable core to the surrounding soil by increasing its thermal conductivity in the vicinity of the cable line [14, 15].

3. Determination of proposed thermal backfill material properties and samples preparation

Thermal backfill mortars are commonly used for enhancing heat dissipation from buried cables to the surrounding soil. Backfill mortars indicate significantly higher thermal conductivity and provide better hydraulic properties compared to the native soil. Thus, in order to provide proper application, the thermal backfill mortar shall exhibit [16]:

- high thermal conductivity over the range of operating conditions,
- low critical moisture content and high thermal stability limits,
- ease of installation with no void spaces existing within the backfill structure,
- low installation and material costs,
- backfill composition based on materials available at the place of installation.

In order to satisfy material properties requirements mentioned above, Fluidized Thermal Backfill (FTB) mortar is widely used in underground cable system installation. Applied in a slurry form, FTB ensures void-free trench filling and results in prolonged moisture retention in a close vicinity of the cable. Therefore, heat transfer from the cable to the surrounding soil enhancement occurs. Thus, air content, naturally trapped in hardened backfill pores, shall not be higher than 2% since its thermal conductivity is significantly lower than for water existing in the hardened backfill pores or solid particles.

In order to ensure proper thermal conditions for UPCS, an efficient thermal backfill material shall be used. In this paper, thermal backfill mixture composed of fine sand and Gruntar^{TM}, mixture designed for extensive use in strengthening and stabilizing ground for the building structures and road embankments, is proposed. Its composition appears to be suitable for the cable bedding application. Gruntar^{TM} is a product of Lafarge Poland – one of the greatest European cement, aggregates and concrete producer [17]. Gruntar^{TM} is an engineered developed mixture which consists mainly of Portland cement, with other mineral additives as fly ash, gypsum, and limestone powder, among others. Gruntar^{TM} is characterized by a high degree of water absorption, high compaction, low shrinkage and suitably selected composition, which allows chemical binding of water.

Proposed thermal backfill mortar is manufactured by mixing fine sand with a specific amount of Gruntar^{TM}. The proportions of Gruntar^{TM} component in backfill material are set as 5, 10 and 15% of mass fraction. Thus, the fine sand constitutes the bulk volume of the mixture while Portland cement and primary Gruntar^{TM} component provide the interparticle bond and proper strength. The proposed backfill mortar is tested for thermal conductivity and its variation with water content.

In cooperation with Lafarge Company, a novel composition of thermal backfill mortar is proposed. Thermal properties of the proposed mortar are comparable to the widely used FTB (Fluidized Thermal Backfill) mortar but of significantly lower cost (~$130 per cubic meter of FTB vs. ~$20 per cubic meter of novel mortar − including only the material costs). Experimental analysis is carried out using Decagon Devices KD2 Pro equipment. During the experiments, the relationship between the water content of the

proposed mortar and its thermal conductivity is determined (such correlations are hard to find in the literature). The thermal conductivity and water content measurements are carried out for the proposed backfill mortar samples. The backfill mortar composition is shown in Table 1.

Table 1 Proposed backfill mortar composition

Mass fraction of Gruntar^{TM}, %	Mass of Gruntar^{TM}, kg	Mass of added water, kg	Mass of quartz sand, kg
5	0.189	0.72	3.6
10	0.40	0.82	3.6
15	0.635	0.74	3.6

As a fine aggregate, which is constituting a bulk volume of the mortar, natural quartz sand is chosen. The considered quartz sand is examined using sieve analysis. The total screen residue on 1.0 mm sieve is 0.2%, on 0.5 mm is 1.1%, on 0.25 mm is 21.2%, on 0.125 mm is 79.3%, and on 0.063 mm is 98.7%.

Investigated backfill mortar was stirred to obtain a uniform structure, and proper samples were formed in cylindrical molds, with a diameter of 110 mm and a height of 200 mm − for thermal conductivity measurements. For moisture content measurements 60g backfill samples were taken from the cylindrical samples before the thermal conductivity measurements.

Thermal conductivity and water content measurements are carried out after 1, 2, 7, 16, 28 and 36 days, counting from the mortar preparation. Throughout the experiment, the samples were stored under normal laboratory conditions at a temperature of 22°C and relative humidity (RH) of 35%. In order to compare the thermal properties of the backfill mortar, measurements were also performed on the pure quartz sand.

The KD2 Pro provided by Decagon Devices® is a fully portable field and lab thermal properties analyzer [18]. KD2 PRO uses the transient line heat source method, described in references [19], [20], [21], to measure the thermal conductivity of solid, liquid and gaseous materials in accordance to ASTM Test Method D5334. The thermal conductivity measurements were conducted using an RK-1 sensor that is recommended for soil, granular materials, concrete, and rocks. The RK-1 sensor accuracy is ±10% in a range from 0.2 – 6.0 W/(m K), and ±0.02 W/(m K) in a range from 0.1 − 0.2 W/(m K). In solid materials, where a pilot hole has been drilled, and contact resistance can be significant, using thermal grease and extending the read time to the maximum allowed 10 minutes is highly recommended, and produce the most accurate results. The mass of water contained in the sample was determined using thermogravimetry method with ± 1.0 mg accuracy. An experimental setup is presented in Fig. 2.

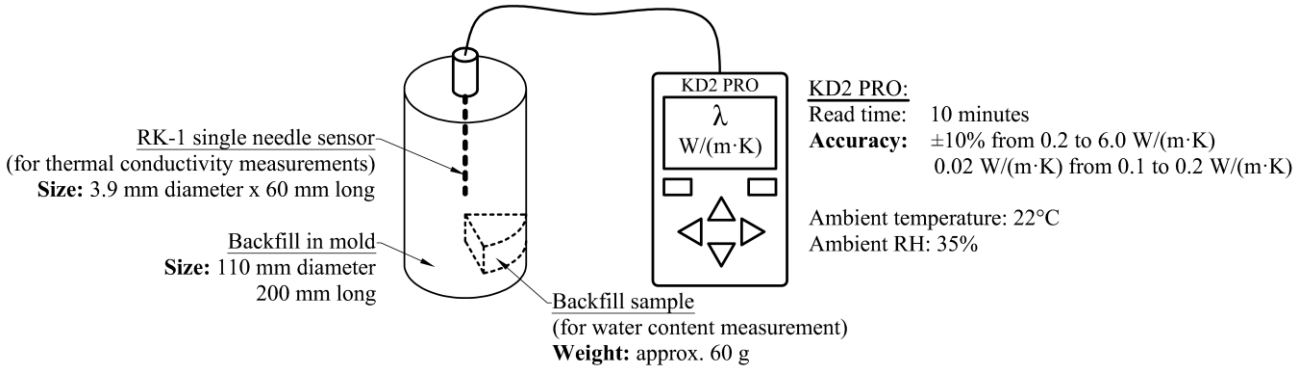

Fig. 2 Experimental setup for measurements of backfill thermal conductivity.

The measurements of backfill thermal conductivity were carried out in the following way. At first, the three samples with 5, 10 and 15% of Gruntar^{TM} mass fraction were prepared . The cylindrical mold with a diameter of 110 mm and a height of 200mm was used during the sample preparation. Water was added to the probes and mixed with sand and Gruntar^{TM} in such a way that the total water content of 15 % was reached, and thermal backfill in a probe was homogeneous. The thermal conductivity was measured at various time levels as presented in Fig. 3. Before each measurement the backfill sample of approx. 60g weight was analyzed to determine water content within the probe. Measurements of moisture content in the backfill sample were conducted using the thermogravimetric method. Losses in the mass of backfill sample were determined during continuous heating at a temperature of 120°C. The sample had been dried until the constant mass from the initial mass $m_{init.}$ to the final mass m_{final} obtained at the end of the sample drying. The measurements were carried out according to ASTM E1582−14 standards [22]. The gravimetric water content w of the sample may be determined as follows:

$$w = \frac{m_{init} - m_{final}}{m_{init}} \cdot 100\% \quad (1)$$

The uncertainty of the sample weight measurement is equal to 1 mg, thus the uncertainty of water content measurement, considering samples with water content lower than 15%, is negligible.

Single series of measurements consisted of thermal conductivity and water content tests during the time when the backfill water content dropped from 15 % to 1 %, that took over 36 days. The measurements series were repeated three times, and the relative difference in measured thermal conductivity was less than 5%. The mean values of thermal backfill conductivity vs time and water content are plotted in Figs 3 and 4.

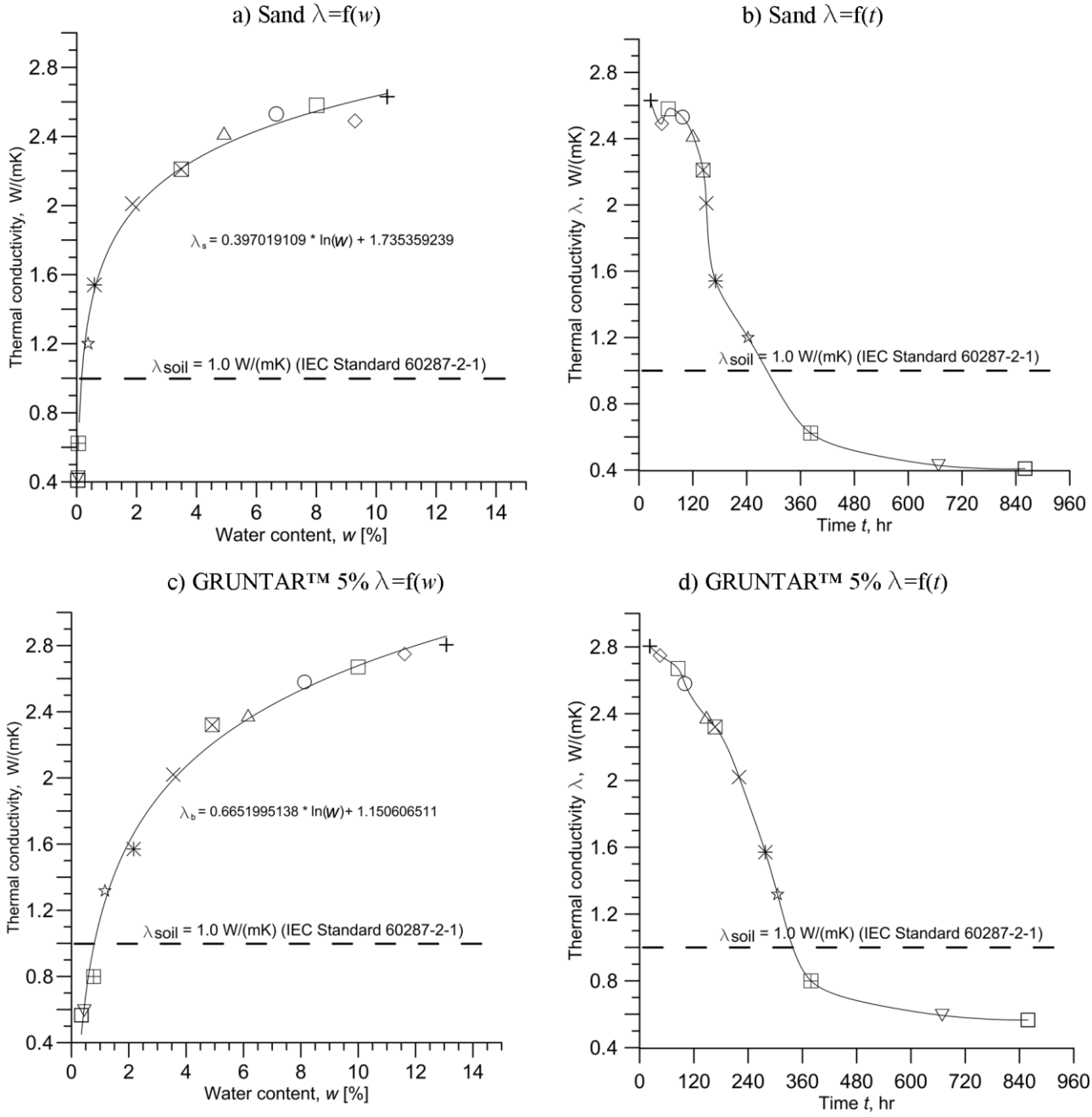

Fig. 3 Thermal conductivity variation of sand and backfill mortar with 5% Gruntar^{TM} mass fraction as a function of water content and time.

Figure 3 shows the results of thermal conductivity measurements for the sand and prepared sand and Gruntar^{TM} mortar (with 5% mass fraction of Gruntar^{TM}) as a function of time and moisture content. Thermal conductivity for fine sand and the backfill mortar is similar in the first days of measurements. After three days the water content in the sand drops significantly. The moisture content drop in the sand probe results in a significant decrease in its thermal conductivity (Fig. 3). After 370 hours, sand is much drier than the proposed backfill mortar. Figure 4presents the thermal conductivity of backfill mortar, with 10% and 15% Gruntar^{TM} mass fraction, as a function of time. For those two thermal backfills, the best values of thermal conductivity were achieved with respect to water content.

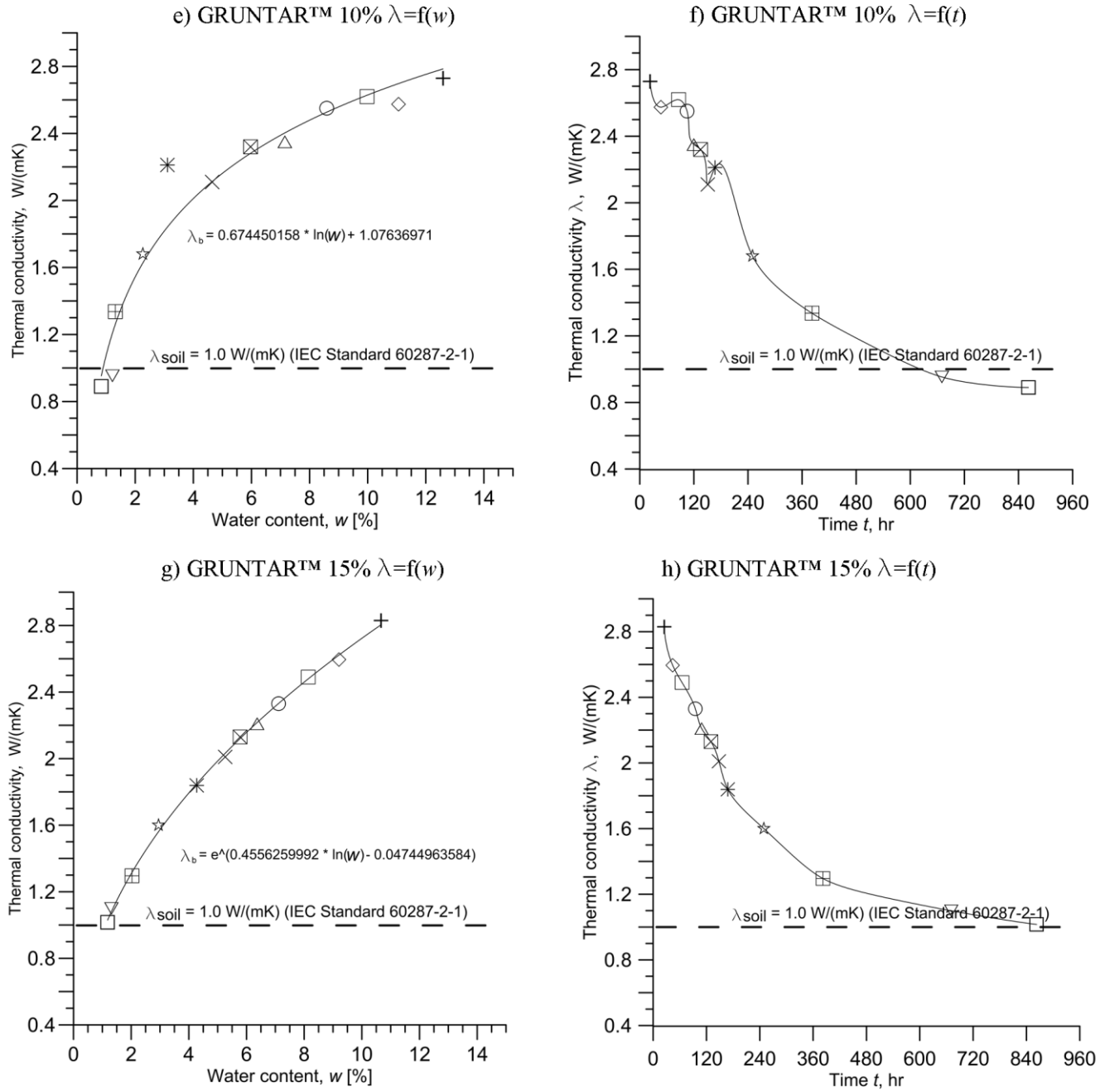

Fig. 4 Thermal conductivity variation of backfill mortar with 10% and 15 % Gruntar^{TM} mass fraction as a function of water content and time.

The experimental value of thermal conductivity as a function of water content and time for backfill mortar with 5%, 10%, and 15 % Gruntar^{TM} mass fraction are the novel contribution of this paper. Such investigations are necessary since the cable engineers need to know how the thermal backfill behaves with a time of operation and changes in water content. IEC Standards [23] provide a thermal conductivity of λ_{soil} = 1.00 W/(m·K) for the native soil for the Polish region. Thermal conductivity of the proposed backfill mortar with 15 % of Gruntar^{TM} mass fraction is significantly higher than 1.00 W/(m·K), as shown in Fig. 4. Even after 6 days (approx. 140h) it exceeds 2.00 W/(m·K). That λ value provides favorable conditions for the underground power cable lines operation. After 36 days thermal conductivity of the hardened backfill mortar (1.18% gravimetric water content) approaches 1.00 W/(m·K), whereas

sand (0.30% gravimetric water content) thermal conductivity drops to 0.40 W/(m·K). Thus, on the basis of the experimental results, it appears that the proposed mortar material provides better heat dissipation conditions than pure quartz sand, especially in dry conditions. Such a value of backfill thermal conductivity allows to maintain the cable core recommended temperature and, hence, to avoid cable line malfunction.

It is also worth of noting, that the assumption of soil thermal conductivity λ_{soil} = 1.00 W/(mK) given by IEC 60287-3-1 [23] for Poland region is a significant simplification. According to the experimental data published by Sepaskhah and Boersma [24], McInnes [25], Campbell et al. [12], as well as Tarnawski and Leong [26] for a soil at low moisture contents and at temperatures ranging from 20°C to 50°C, soil thermal conductivity varies from 0.20 to 1.40 W/(m·K). The thermal conductivity of a soil depends strongly not only on water content, but also depends on temperature, bulk density, and soil composition. Speaking of the soil thermal conductivity, without specifying the water content, bulk density, temperature, and composition, is meaningless. The behavior of soil thermal conductivity with varied water content, temperature and clay content is well described by Campbell - de Vries model and will be discussed in section 5. The density of soil varies with its composition which in turn drastically changes with geographical location. For a soil occurring in a particular place the composition and density are fixed, and the temperature typically varies over a small range, so that, have a little effect on soil thermal conductivity. Thus, the main variable for soil in place is, therefore, moisture content [24]. Nevertheless, a common practice among an HV power cables producers is to assume fixed thermal conductivity and soil temperature values when selecting power cables to their clients. Such a guidelines are given in the international standard IEC 60287-3-1 [23]. Thus, it appears that such a considerable simplification do not reflect the actual burial conditions.

The UPCS thermal performance optimization is performed for the 400kV underground power cable system, for which the proposed thermal backfill is applied. In a present study, the system of three 400kV cables arranged in flat formation is considered. The power cables are laid in Polyethylene (PE) conduits filled with sand-bentonite-based buffer material with a dry density of 1700 kg/m^3 and thermal conductivity of 0.95 W/(m·K) [27]. The PE conduits are situated in thermal backfill with a 15% of Gruntar^{TM} mass fraction. The external diameter and thickness of PE casing pipe are 278 mm and 14 mm, respectively. The mixture proposed by [27] is composed of MX-80 (Na-bentonite), sand and water. Sand mass fraction and water contents are 37.5% and 8.17%, respectively [27].

4. Mathematical model of heat transfer in UPCS

The recently performed studies on UPCS and soil heat and mass transfer include both the experimental [28] and numerical [29], [30], [31], [32], [33], [34] approaches. One of the most efficient methods for thermal analysis of UPCS is the Finite Element Method. This section presents the fundamental equations used in the modeling of heat transfer processes in UPCS.

The heat transfer problem, related to the studied UPCS, is considered as two-dimensional and steady-state. The Cartesian coordinate frame was employed instead of cylindrical since the ground and backfill layer domain are of rectangular shape. Also, from a view of Finite Element programming, it is more efficient to use dense triangular Finite Elements mesh than a mesh with specialized isoparametric Finite Elements applied for the cylindrical coordinate system. The Finite Element Method (FEM) code developed in MATLAB is used to solve the heat conduction equation [33]:

$$\frac{\partial}{\partial x}\left[\lambda(T)\frac{\partial T}{\partial x}\right]+\frac{\partial}{\partial y}\left[\lambda(T)\frac{\partial T}{\partial y}\right]=-q_v(T_c) \tag{2}$$

In Eq. (2) T denotes the temperature at any point in the x-y plane around the underground cable; λ represents the thermal conductivity (note the dependence of thermal conductivity on temperature), and $q_v(T_c)$ is a temperature dependent volumetric heat source per cable core unit volume, defined as:

$$q_v(T_c)=\frac{\Delta Q}{A_c} \tag{3}$$

where A_c denotes the cable conductor cross-sectional area. The value of A_c is calculated as $A_c = 0.25\pi d_c^2$ while ΔQ is the cable heat loss (computed from the first Joule's law). The method of determining q_v uses the simplified geometrical model of 400kV XLPE single core underground power cable (Fig. 5a) buried at the depth of H under the ground level (Fig. 5b).

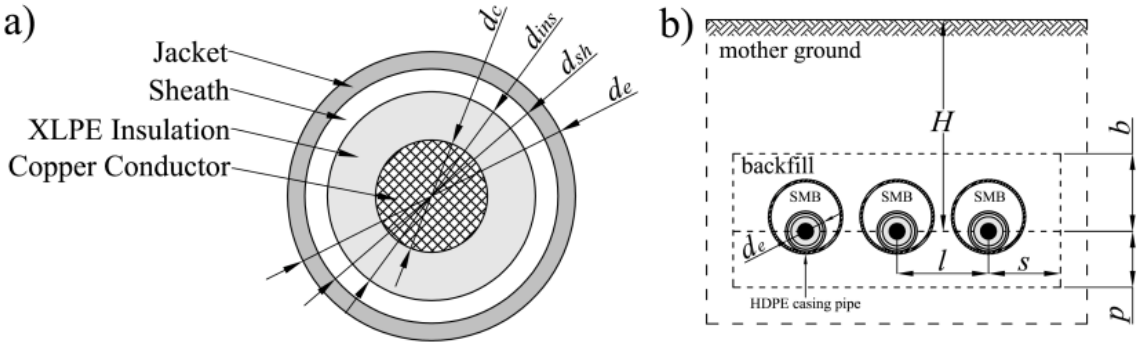

Fig. 5 Simplified model of a) 400kV underground power cable considered for the determination of volumetric heat transfer rate q_v; b) the geometrical arrangement of the considered transmission line.

Table 2 lists the materials and thermal conductivities of the individual cable layers shown in Fig.5a.

Table 2 Thermal properties and thicknesses of 400kV power cable layout materials and casing pipe [34]

Cable layer	Material	Diameter, mm	Thermal conductivity, W/(m K)
Conductor	Copper	d_c= 49.6	400.00
Insulation	XLPE	d_{ins}= 110.6	0.2875
Sheath	Copper	d_{sh}=123.0	400.00
Jacket	HDPE	d_e=133.6	0.2875
Casing pipe	PE	d_{in} = 250 d_{out} = 278	0.45

Heat losses in the power cable are expressed by Joule's law by introducing current rating I and alternating current (AC) electric resistance $R_{e,AC}$ to the equation:

$$\Delta Q = I^2 R_{e,AC} \tag{4}$$

This paper considers the constant value of current rating I = 1145 A, which is given by cable producer [13], due to consideration of to steady-state operational conditions. The current loading is provided at a nominal temperature of 65°C.

The considered cable core DC resistance, given at reference temperature 20°C, is $R_{e,DC}$ = 0.0113 Ω/km. Furthermore, AC resistance, given at the nominal cable core temperature equal to 65°C, is $R_{e,AC}$ = 0.0157 Ω/km.

Losses in the cable conductor are affected by current concentrating near the conductor surface (skin effect) during the current flow and also by a magnetic field, induced in neighboring cables, affecting the distribution of current across the conductor (proximity effect) [16]. Skin and proximity effect coefficients y_s and y_p [35] are calculated, respectively as:

$$y_s = \frac{x_s^2}{192 + 0.8x_s^2}, \qquad x_s = \frac{8\pi f}{R_{e,DC}} 10^{-7} k_s \tag{5}$$

$$y_p = \frac{x_p^2}{192 + 0.8x_p^2}\left(\frac{d_c}{l}\right)^2 \left[0.312\left(\frac{d_c}{l}\right)^2 + \frac{1.18}{\frac{x_p^2}{192 + 0.8x_p^2} + 0.27}\right], \quad x_p = \frac{8\pi f}{R_{e,DC}} 10^{-7} k_p \tag{6}$$

where k_s and k_p are skin and proximity effect correction factors, equal to 0.435 and 0.37, respectively, for the case of segmented conductor type [36]. In Eq. (5) and Eq. (6), f = 50 Hz is an alternating current frequency and l is a distance between adjacent conductor axes.

Cable conductor resistance exhibits a greater electric resistance in the case of alternating current flow

($R_{e,AC}$) than for direct current ($R_{e,DC}$). Skin and proximity effects that mainly cause the observed changes may be introduced to Eq. (4) by using y_s and y_p, respectively:

$$R_{e,AC} = R_{e,DC}(1 + y_s + y_p) \tag{7}$$

Cable conductor temperature, affected by the heat dissipation conditions, also exhibits a significant influence on conductor DC electrical resistance:

$$R_{e,DC} = R_{e,ref}\left[1 + \alpha_{\text{ref}}(T_{c,FEM} - T_{ref})\right] \tag{8}$$

where, $R_{e,ref}$, and $\alpha_{e,ref}$ are the reference cable conductor's electric resistance, and the temperature coefficient for the conductor material, both given at the reference temperature T_{ref} = 20°C. The cable conductor temperature determined from Eq. (2) using the FEM model of underground power cable system is denoted as $T_{c,FEM}$ and is given in °C. For the described computational cases (braided copper conductor) it is assumed that $R_{e,ref}$ = 0.0113 Ω/km and $\alpha_{e,ref}$ = 0.00393 (according to [13]).

The operating conditions for the considered power transmission line assume maximum current loading as 1145A. Therefore, this study considers q_v function (Eq. (3)) determined for a given value of I = 1145 A. The FEM method is used to discretize and solve Eq. (2) in a similar manner as presented in [34]. Also, the literature references [34], [37], [38], [39], [40], [41] present the application of Finite Element Method for analysis of underground power cable systems.

5. Soil thermal conductivity model

Eq. (2) requires specifying the thermal conductivity of all considered heat transfer media: cable core, insulation, applied thermal backfill mortar and surrounding soil. The thermal conductivities of the first three media are specified in the previous sections. Due to the complexity of soil heat and mass transfer, determination of soil thermal conductivity requires a comprehensive model, as presented by Bittelli et al. [42], [43]. The soil thermal conductivity model, used in this study, was published by Campbell et al. [12] and it is a modification of the original de Vries [44] model. The model is based on the assumption that the thermal conductivity of the material is given by a weighted sum of the thermal conductivities of its components:

$$\lambda = \frac{k_w \theta \lambda_w + k_s \phi_s \lambda_s + k_g \phi_g \lambda_g}{k_w \theta + k_a \phi_s + k_m \phi_g} \tag{9}$$

where k_g, k_s and k_w are weighting factors for gas, solid and water. λ is the soil thermal conductivity and λ_g, λ_s and λ_w are thermal conductivities for gas, solid and water. The volumetric fractions of gas, solid and water are ϕ_g, ϕ_s and θ. The thermal conductivity of the gas phase accounts for both the conductivity of air (λ_a) and the latent heat component given by evaporation and condensation. In most soil models, thermal conductivity is considered to be independent of temperature. However, Campbell et al. [12] showed that λ is temperature dependent, and the dependence is mostly due to the variation of the latent

heat transport with temperature. With respect to the de Vries [44] model, the model of Campbell et al. [12] provides a more rational treatment of the transition from high to low vapour contributions as the soil dries. Indeed, the de Vries [44] model accounted for the thermal conductivity of continuous phases: when the soil is saturated the continuous phase is the liquid water and when the soil is dry, the continuous phase is gas. However, the de Vries [44] model did not account for the average conditions of partial saturation occurring in soils. This was introduced by Campbell et al. [12] by defining a continuous function through the "fluid" thermal conductivity variable that can be used over the whole range of water contents. The authors defined a variable called "fluid" thermal conductivity:

$$\lambda_f = \lambda_g + f_w \left(\lambda_w - \lambda_g \right) \tag{10}$$

where f_w is an empirical parameter computed by:

$$f_w = \frac{1}{1 + \left(\frac{\theta}{\theta_o} \right)^{-q}} \tag{11}$$

ranging from 0 in dry soil to 1 in saturated soil. The parameters θ_o and q are specific material properties that determine when water content begins to affect thermal conductivity and the rate of the transition from air to water dominated conductivity. The parameters q and θ_o are found to be highly correlated to clay content, and the following regression equations were presented:

$$q = 7.25 m_y + 2.52 \tag{12}$$

and

$$\theta_O = 0.33 m_y + 0.078 \tag{13}$$

where m_y is the fractional clay content, and $0 \le m_y \le 1$.

The weighting factors are then computed:

$$k_g = \frac{1}{3} \left[\frac{2}{1 + g_a \left(\frac{\lambda_g}{\lambda_f} - 1 \right)} + \frac{1}{1 + g_c \left(\frac{\lambda_g}{\lambda_f} - 1 \right)} \right], \tag{14}$$

$$k_s = \frac{1}{3} \left[\frac{2}{1 + g_a \left(\frac{\lambda_s}{\lambda_f} - 1 \right)} + \frac{1}{1 + g_c \left(\frac{\lambda_s}{\lambda_f} - 1 \right)} \right], \tag{15}$$

$$k_w = \frac{1}{3} \left[\frac{2}{1 + g_a \left(\frac{\lambda_w}{\lambda_f} - 1 \right)} + \frac{1}{1 + g_c \left(\frac{\lambda_w}{\lambda_f} - 1 \right)} \right], \tag{16}$$

where g_a and g_c are the shape factors. The value of g_a for mineral soils is 0.088 and $g_c = 1 - 2g_a$. Therefore,

it is sufficient to obtain only one shape factor.

The thermal conductivity of the gas phase λ_g is given by:

$$\lambda_g = \lambda_a + \frac{L_\upsilon \Delta f_w \rho D_\upsilon}{P - e_a} \tag{17}$$

where λ_a is the thermal conductivity of air, L_υ is the latent heat of vaporization, Δf_w is the slope of the saturation vapour pressure function, D_υ is the vapour diffusivity for soil, ρ is the molar density of air, P is the atmospheric pressure, and e_a is the actual vapour pressure. The second term is the latent heat term and is responsible for almost all the temperature dependence of soil thermal conductivity.

Fig. 6 shows the behavior of Campbell – de Vries model of soil thermal conductivity for soil bulk density of 1220kg/m^3 while clay content varied in the range from 0.2 to 0.8. The soil water content ranged from 0.05 (parched soil) to 0.4 (wet soil), and the ground temperature changed from 20°C to 100°C.

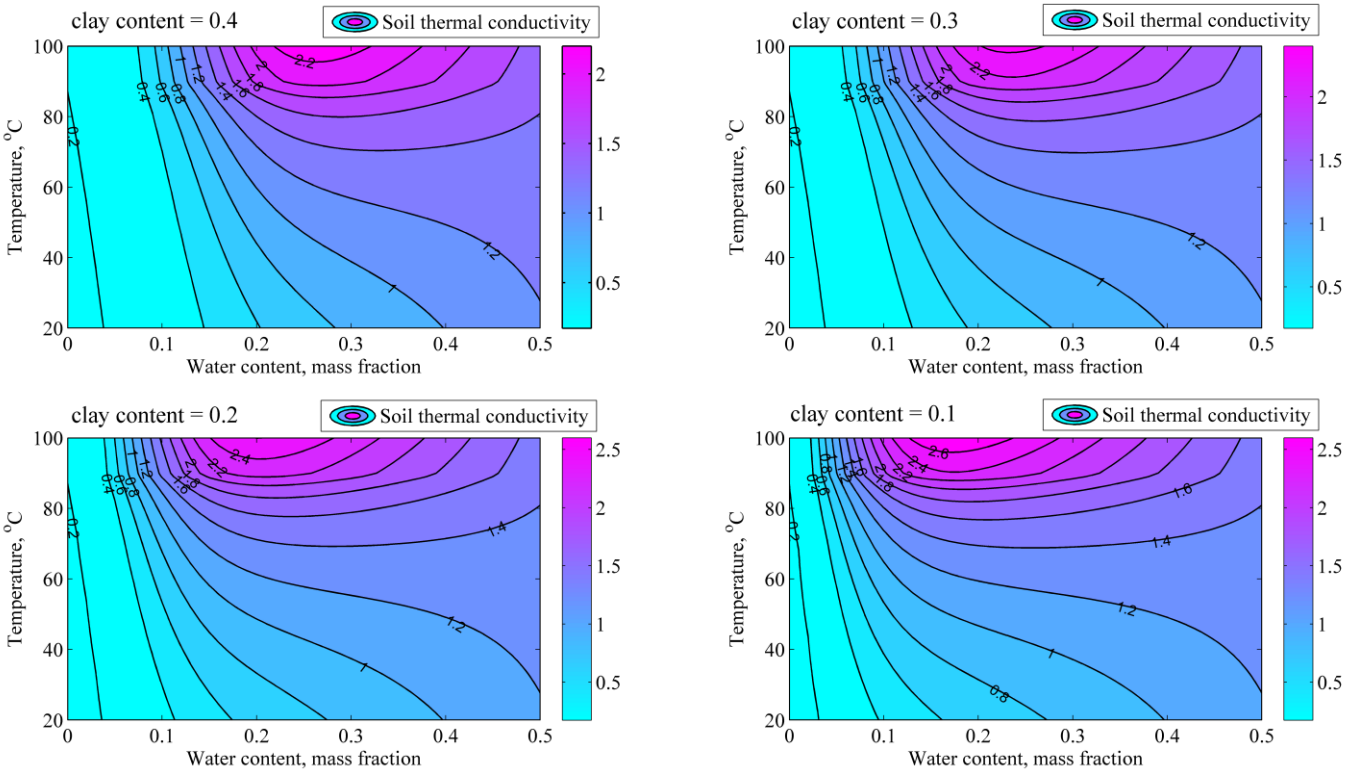

Fig. 6 Soil thermal conductivity (in W/ (m K)) calculated from Campbell – de Vries model for different values of soil water content, temperature, and clay content. The bulk density of soil was assumed as 1220 kg/m^3.

In Fig. 6 one can see the following behavior of Campbell – de Vries model:

- soil thermal conductivity rises with an increase in temperature. However, when the clay content is growing, soil thermal conductivity demonstrates lower temperature dependence.
- soil thermal conductivity decreases with the decrease in moisture content.

Since the proportion of the soil components varies with space and time, the thermal conductivity of

soil depends on properties that vary with space and time such as its bulk density, water content, quartz content and organic matter content. At low water content, the airspace controls the thermal conductivity. At high water content, the thermal conductivity of the solid phase becomes more important. The thermal conductivity of pure water is temperature dependent (water thermal conductivity increases with temperature), therefore with increasing water content in the porous material, the bulk thermal conductivity increases. However, this is not the most important process.

The large differences in thermal conductivity among different materials are the result of differences in bulk density and composition. The transition from low to high conductivity occurs at low water content in sands and at high water content in soils high in clay. In particular, the temperature dependence of thermal conductivity is mostly due to the variation of the latent heat transport with temperature. When the soil is not saturated with water, the gas phase is at variable values of water vapor pressure. Therefore, the movement of water vapor is driven by differences in vapour concentration and by thermal gradients [43]. When temperature increases the transport of latent heat increases as well since the saturation vapor pressure increases with temperature. At the pore scale, thermal conductivity is affected by both sensible heat transport (conduction between solid particles) and by latent heat transport (convection associated with the transport of latent heat).

The computations presented in this paper consider the following parameters of soil, used as the input to Campbell – de Vries model [43], [45], [46]:

- soil bulk density of 1220 kg/m^3,
- soil water content of 0.2,
- clay content of 0.4.

The conditions correspond to the silty sand soil; the assumed water content corresponds to the summer time period. It is also assumed that the backfill mortar material is not entirely dry, with the gravimetric fraction of water equal to 5%. Thus, the corresponding thermal conductivity is equal to 2.35 W/(m K). The value of soil water content equal 0.2 corresponds the unfavorable conditions during summer when the soil water content may drop from 0.4-0.3 to 0.2 or even lower.

6. Momentum-type particle swarm optimization

PSO algorithm is a widely used optimization tool. It is characterized by a low computational cost and is easy to use in various scientific and engineering applications. Campana et al. [47] considered the evolutionary PSO-algorithm for the minimization of a computationally costly nonlinear function, in global optimization frameworks. By using an open-loop model for a dynamic linear reformulation of PSO iteration, the authors had provided the general conditions in order to avoid possibly diverging paths of the particles.

For most popular optimization problems which are defined in the discrete space, Beheshti [48] proposed the Binary Accelerated Particle Swarm Algorithm (BAPSA) with global and local topologies.

The goal of the algorithm was to accelerate the learning and convergence procedure of classifiers.

Kaucic [49] presented a multi-start PSO-algorithm for the global optimization of a function subject to bound constraints. The novelty of the procedure was the integration of the opposition-based computing into a PSO with an adaptive velocity used in order to produce some additional exploration ability of the search space.

The momentum-type PSO algorithm was developed by Liu and Lin [50]. The algorithm uses the delta momentum term (Δv_i^n) in the formula of the particle velocity, and beta parameter (β). In their study, the authors confirmed the better convergence of algorithm when compared to the classical PSO method [51], [52], [53]. Due to the ease of implementation and quite good convergence behavior, this algorithm is applied in the present study.

Eqs (18) – Eq. (20) define the nonlinear constrained optimization problem [50]:

Minimize $$f(\mathbf{x}), \quad \mathbf{x} = [x_1, x_2, ..., x_N] \in R^N \tag{18}$$

Subject to $$g_j(\mathbf{x}) \le 0 \quad , j=1,\ldots,p \tag{19}$$

$$h_j(\mathbf{x}) = 0 \quad , j=p+1,\ldots,m \tag{20}$$

where $\mathbf{x}$ is a vector of design variables, $f(\mathbf{x})$ is an objective (cost) function in N_{dim} hyperspace, when $g_j(\mathbf{x})$ and $h_j(\mathbf{x})$ represents the inequality and equality constrained functions. The numbers of inequality and equality constraints are given as p and $m - p$, respectively.

This study employs the momentum–type Particle Swarm Optimization (PSO) algorithm [50] and a dynamic penalty function with a continuous assignment to solve nonlinear constrained global optimization problem. The PSO algorithm is inspired by the social behavior simulation for groups of organism, such as flocks of birds and schools of fish. The particles represent the sets of design variables. The particle swarm with size N_{par} is defined during the initial iteration. The particle velocity determines its position in the successive iteration. The algorithm finds the global minimum of $f(\mathbf{x})$ if the particle position is the same for all particles in the swarm, or the other specified convergence criterion is satisfied. The momentum–type PSO algorithm uses only two equations, first for the velocity of an i–th particle in n–th iteration $\mathbf{v}_i^n$ and the second for the new position of the particles $\mathbf{x}_i^n$.

The general form of the equation for an i-th particle velocity $\mathbf{v}_i^n$ is given as follows [50]:

$$\mathbf{v}_i^n = \beta \times \Delta \mathbf{v}_i^{n-1} + c_1 \times rand() \times (pbest_i - \mathbf{x}_i^{n-1}) + c_2 \times rand() \times (gbest_i - \mathbf{x}_i^{n-1}) \tag{21}$$

The particle position $\mathbf{x}_i^n$is updated in the following manner:

$$\mathbf{x}_i^n = \mathbf{x}_i^{n-1} + \alpha \times \mathbf{v}_i^n, \; i = 1, 2, ..., N_{par} \tag{22}$$

Equation (22) allows dynamic self–adaptation of each particle in the search space over time. The i–th particle can memorize the previous velocity variation state and automatically adjust the next velocity value during movement. The delta momentum term in the PSO algorithm $\Delta \mathbf{v}_i^{n-1} = \mathbf{v}_i^{n-1} - \mathbf{v}_i^{n-2}$stabilizes

searching, and an appropriate value for β improves the convergence and optimal solution. In a particle velocity formula, given by Eq. (21), *rand()* is a random number between 0 and 1. The momentum constant β is equal to 0.1 as proposed in [50]. The initial condition for Δv_i^{n-1} assumes its value equal to zero, i.e. $\Delta \mathbf{v}_i^0 = 0$. The parameter α_{PSO} is set to 1 in this work as suggested in ref. [50]. Therefore, the variables are interpreted as an actual velocity, i.e. the change between two successive particle positions [51]. The particle interaction parameters c_1 and c_2 are both equal to 2. In a state of equilibrium, other particles are not able to find better positions, i.e. $\mathbf{x}_i^n = pbest_i$ and $\mathbf{x}_i^n = gbest_i$ where *pbest* denotes the best particle position and *gbest* is the global best position. The converged solution ensures that Eq. (21) satisfies the zero velocity variation ($\Delta \mathbf{v}_i^{n-1} = 0$) and zero velocity ($\mathbf{v}_i^n = 0$) conditions for the considered particle.

This study employs the dynamic penalty function, as suggested in [50]. An active function $C(n)$ and a continuous assignment function $H(\mathbf{x})$ handle the linear and nonlinear constraints:

$$F(\mathbf{x}) = f(\mathbf{x}) + C(n)H(\mathbf{x}) \tag{23}$$

where $f(\mathbf{x})$ represents the original objective function of the constrained problem (Eq. (18)); $C(n)$ denotes a dynamically modified penalty value dependent on the iteration number n; $H(\mathbf{x})$ is a penalty factor. The terms $C(n)$ and $H(\mathbf{x})$ for m linear and nonlinear constraint $g_j(\mathbf{x})$ (Eqs (19−20)) are given as [50]:

$$C(n) = (c_{pf} \times n)^{\alpha_{pf}} \tag{24}$$

$$H(\mathbf{x}) = \sum_{j=1}^{m} \left[\theta(q_j(\mathbf{x})) \times q_j(\mathbf{x})^{\gamma(q_j(\mathbf{x}))} \right] \tag{25}$$

$$\theta(q_j(\mathbf{x})) = a_{pf} \times \left(1 - \frac{1}{e^{q_j(\mathbf{x})}} \right) + b_{pf} \tag{26}$$

where $q_j(\mathbf{x}) = \max\{0, q_j(\mathbf{x})\}$, $j = 1,...,m$, so that, when q is negative then it is considered as 0. The function $q_j(\mathbf{x})$ is a relative violated function of the constraints, $\theta(q_j(\mathbf{x}))$ denotes a continuous assignment function of exponential type, and $\gamma(q_j(\mathbf{x}))$ defines the power of the violated function. The constants for Eqs (24) – (26) are selected as [13]: $c_{pf} = 0.5$, $\alpha_{pf} = 2$, $a_{pf} = 150$, and $b_{pf} = 10$. If $q_j(\mathbf{x}) \leq 1$, then the power $\gamma(q_j(\mathbf{x})) = 1$; in the other case $\gamma(q_j(\mathbf{x})) = 2$, as given in [50].

6.1. Optimization problem formulation

This study applies the momentum-type PSO for minimizing the cross-sectional area A_b of backfill mortar layer. It should be noted that A_b is only a half of the real backfill cross-sectional area. Moreover, the physical geometry of the modeled underground power cable system and the expected pattern of the thermal solution exhibits mirror symmetry. Fig. 7 shows the decision (design) variables *l*, *s*, *p* and *b*, where:

- *l* is the horizontal distance between the cable conductors axes,
- *s* is the spacing between the right edge of the bedding layer and the side cable axis,

- *b* is the distance between the conductors axes and the top of the bedding layer,
- *p* is the distance between the conductors axes and the bottom of the bedding layer.

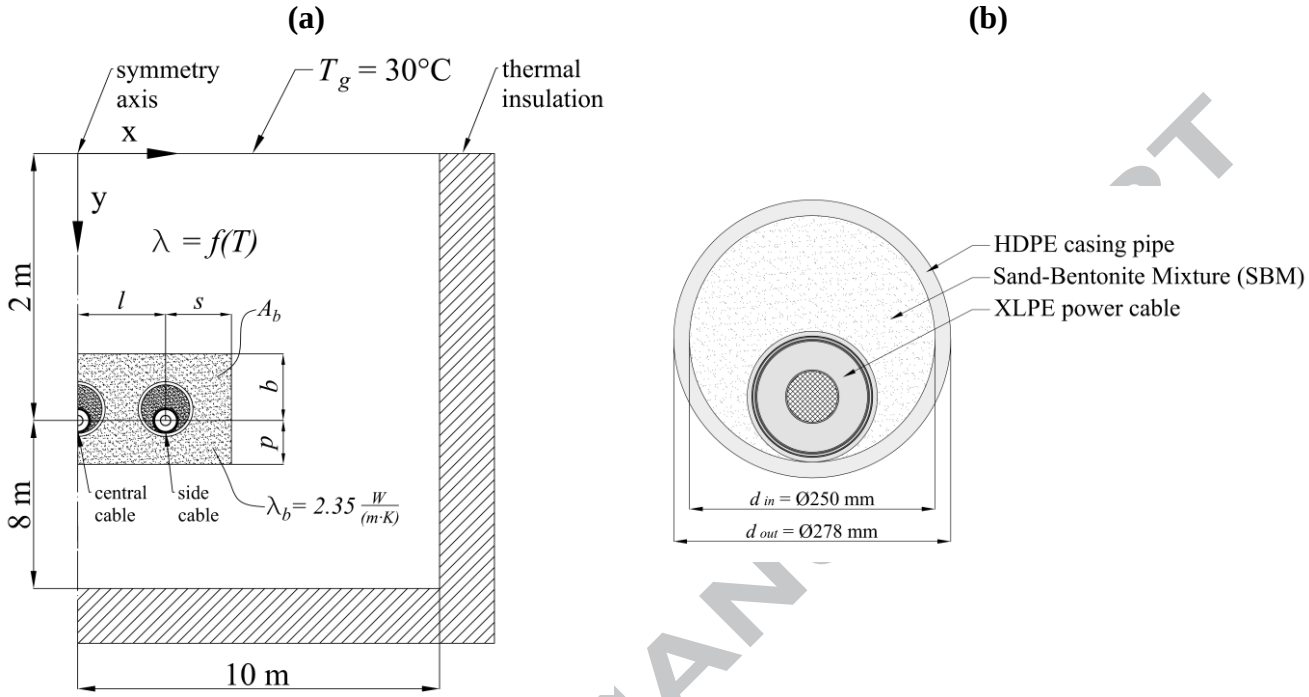

Fig. 7 Flat formation arrangement of underground power cable system considered for the optimization procedure. (a): the physical geometry of the modeled underground power cable system; (b): power cable placed in an HDPE casing pipe.

The real system of underground electrical energy transmission line consists of three power cables. The cables are located at depth *H* of 2.0 m below the ground level. However, due to the expected mirror symmetry of the temperature field solution pattern, only the half of the real system is modeled. The square domain with height and width of 10.0 m is used in the computations. It is assumed that the right, left and bottom edges of the boundary region are thermally insulated (i.e. no heat flow exists in a direction perpendicular to the domain edge). The size of the computational domain with a width of 10.0 m and a height of 10.0 m was used since further increase in domain dimensions has a negligible effect on cable core temperature. In contrary, the decrease in domain dimensions, both height and width from 10.0 m to 5.0 m leads to the increase in cable core temperature up to 2ºC for the computational case assumed in this paper. It is also possible to consider the given temperature distribution at the right boundary (the temperature may be determined based on the measurement data [57]). The insulation boundary conditions assume no heat reception; therefore, the ground temperature is higher than in the case when temperature distribution based on [57] is applied. From the data in [57] one can observe that the mean temperature in July is approx. 31 ºC at a depth of 2 cm, 22 ºC at a depth of 0.5 m, 17.2 ºC at a depth of 2 m, 12.5 ºC at a depth of 4 m and 10.2 ºC at a depth of 12 m. Of course, those temperatures can slightly vary depending on the climate zone, however for Poland and Germany region may be assumed similar. The assumption of thermally insulated sides of the domain (bottom and right edge) leads to the ground temperature in heat

transfer domain higher than 30 ºC (Fig. 11). As a result, when insulation boundary condition is applied at domain sides, the cable core temperature is up to 5ºC higher (for the computational case performed) when compared to the case of given temperature distribution based on [57]. Therefore, the assumed insulation boundary condition provides a safety margin for thermal design of UPSC. At the top edge (the ground level), the temperature T_g is set to 30°C and is 5°C higher than in ref. [54] due to the possible adverse conditions of heat dissipation in summer time period. Eq. (27) summarizes the boundary conditions applied when solving Eq. (2):

$$\begin{aligned}
&\left.\frac{\partial T}{\partial x}\right|_{x=10\text{m}} = 0, \quad \text{for the boundary region right edge,}\\
&\left.\frac{\partial T}{\partial x}\right|_{x=0} = 0, \quad \text{for the symmetry plane,}\\
&\left.\frac{\partial T}{\partial y}\right|_{y=10\text{m}} = 0, \quad \text{for the boundary region botom edge,}\\
&T(x, y=0) = T_g = 30°\text{C}, \quad \text{for the boundary region top edge.}
\end{aligned} \tag{27}$$

The heat conduction equation describes the mathematical model of heat transfer processes (Eq. (2)) with the non−linear (temperature dependent) source term (Eq. (3)). The boundary conditions for Eq. (2) are given by Eq. (27). The calculation method for determining the source term is given by Eqs (4 –8). The most significant heat transfer barrier is a native soil and a thermal backfill layer. To calculate the soil thermal conductivity, required by Eq. (2), the comprehensive Campbell – de Vries model (Eqs (9 – 17)) is used. The heat conduction equation (Eq. (2)) is discretized using the Finite Element Method (FEM) and solved employing the Jacobi scheme. The solution here is the nodal temperature distribution in the entire cable system. The maximum value of determined temperature (T_{cmax}) is considered in solving the optimization problem (Eqs 28– 29).

The algorithm for FEM simulations of UPCS was presented by the authors of this paper in the previous study [33]. In Appendix A of that paper, the detailed algorithm of FEM simulations was given. Also, the FEM codes (written in MATLAB) for UPCS analysis were attached in Appendix B. The codes were listed in the supplementary material section. This paper uses the FEM solver developed in [34], but the emphasis is not on FEM simulation but on optimization of UPCS.

Eqs (28) and (29) define the optimization problem for the underground cable system (Fig. 6):

$$\text{Minimize} \qquad F(\mathbf{x}) = A_b(\mathbf{x}) + C(n)H(\mathbf{x}), \quad \mathbf{x} = [l,\, s,\, p,\, b] \in R^4 \tag{28}$$

$$\text{Subject to} \qquad q_j(\mathbf{x}) \le 0, \quad j = 1 \tag{29}$$

$$\text{with } q_j(\mathbf{x}) = T_{c\max}(\mathbf{x}) - T_{opt},$$

where T_{opt} is the best-found operation temperature of the cable conductor i.e. T_{opt} = 65°C and $T_{c\ \max}(\mathbf{x})$ denotes the maximum cable conductor temperature, determined for the **x** vector of design variables. It should be noted that the number of function constraints *j* is equal to 1 since only the constraint is that the

$T_{c\ \max}(\mathbf{x})$ temperature shall not exceed the T_{opt} value. In FEM simulations, the discrete model of underground power cable system is created based on the values of design variables specified by a vector **x**. The $T_{c\ \max}(\mathbf{x})$ temperature is determined by the location of central cable conductor gravity center (Fig. 6), from FEM simulations. The constraints on design variables are assumed as:

$$\begin{aligned} 0.3 \le\ & l \le 0.6 \\ 0.2 \le\ & p, b, s \le 0.6 \end{aligned} \tag{30}$$

For the given number of particles in swarm N_{par}, the $T_{c\ \max}(\mathbf{x}_i)$ temperatures and the corresponding FTB bedding layer cross-sectional areas $A_b(\mathbf{x}_i)$ are determined for each particle position $\mathbf{x}_i$; i= 1,...,N_{par}. As a result, the objective function $F(\mathbf{x}_i)$ can be evaluated for all particles. Then the momentum−type PSO optimization procedure is applied to solve the constrained optimization problem given by Eqs (28)-(30). The x and y denote the Cartesian coordinate axes that are used to create the geometrical model of UPCS employed in Finite Element Simulations. Note, that **x** = [l, s, p, b] is a vector of decision (design) variables, but x is the Cartesian coordinate.

The optimization problem expressed by Eqs (28)−(30) is further explained below:

- A_b(**x = [**l, s, p, b**]**) - the area of backfill layer. The area is calculated from the FEM model of UPCS as a sum of finite element areas in the backfill layer domain. The decision variables are l, s, p and b (shown in Fig. 6). The cable backfill area is minimized during the optimization.
- C(n), evaluated from Eq. (24), denotes a dynamically modified penalty function dependent on the iteration number n;
- H(**x** = [l, s, p, b]) is a penalty factor. To calculate the value of H(**x** = [l, s, p, b]), the value of q(**x = [**l, s, p, b**]) =** $\boldsymbol{T}_{cmax}$**(x** = [l, s ,p, b]) – T_{opt} is needed to be determined. The maximum temperature of cable core $\boldsymbol{T}_{cmax}$ is calculated as the maximum temperature value determined from FEM model of UPCS. The FEM model allows defining the discrete form of heat conduction equation, which is then solved using the Jacobi iteration method. The solutions of FEM are the nodal temperatures. The best-found cable core temperature is T_{opt} = 65°C as defined by the cable producer. The number of functional constraints is m = 1 since only the constraint is that the maximum temperature of cable core shall be lower than the best-found cable core temperature, $\boldsymbol{T}_{cmax}$**(x** = [l, s, p, b]) – T_{opt} < 0. The constraint on cable core temperature is implied as a dynamic penalty function in the definition of the cost function Eq. (28).

It is assumed that the algorithm convergence is achieved if the convergence criterion ε<0.0001 is satisfied:

$$\begin{aligned} &\boldsymbol{\delta}^n = \left[\ \delta_1^n,\ \delta_2^n,....,\ \delta_{N_{par}-1}^n, \delta_{N_{par}}^n\ \right] = \left[\ \left|\mathbf{v}_1^n\right|,\ \left|\mathbf{v}_2^n\right|,....,\ \left|\mathbf{v}_{N_{par}-1}^n\right|, \left|\mathbf{v}_{N_{par}}^n\right|\ \right], \\ &\varepsilon = \max(\boldsymbol{\delta}^n) < 0.0001. \end{aligned} \tag{31}$$

In Eq. (31), δ_i^n is equal to the magnitude of the $\mathbf{v}_i^n$ vector. The values of $\delta_i^n$are determined for all

particles existing in a swarm, i.e. i= 1,..., N_{par}. The maximum value of $\boldsymbol{\delta}^n$ components, i.e. ε, shall not exceed 0.0001.

The flowchart of the computational algorithm is shown in Fig. 8.

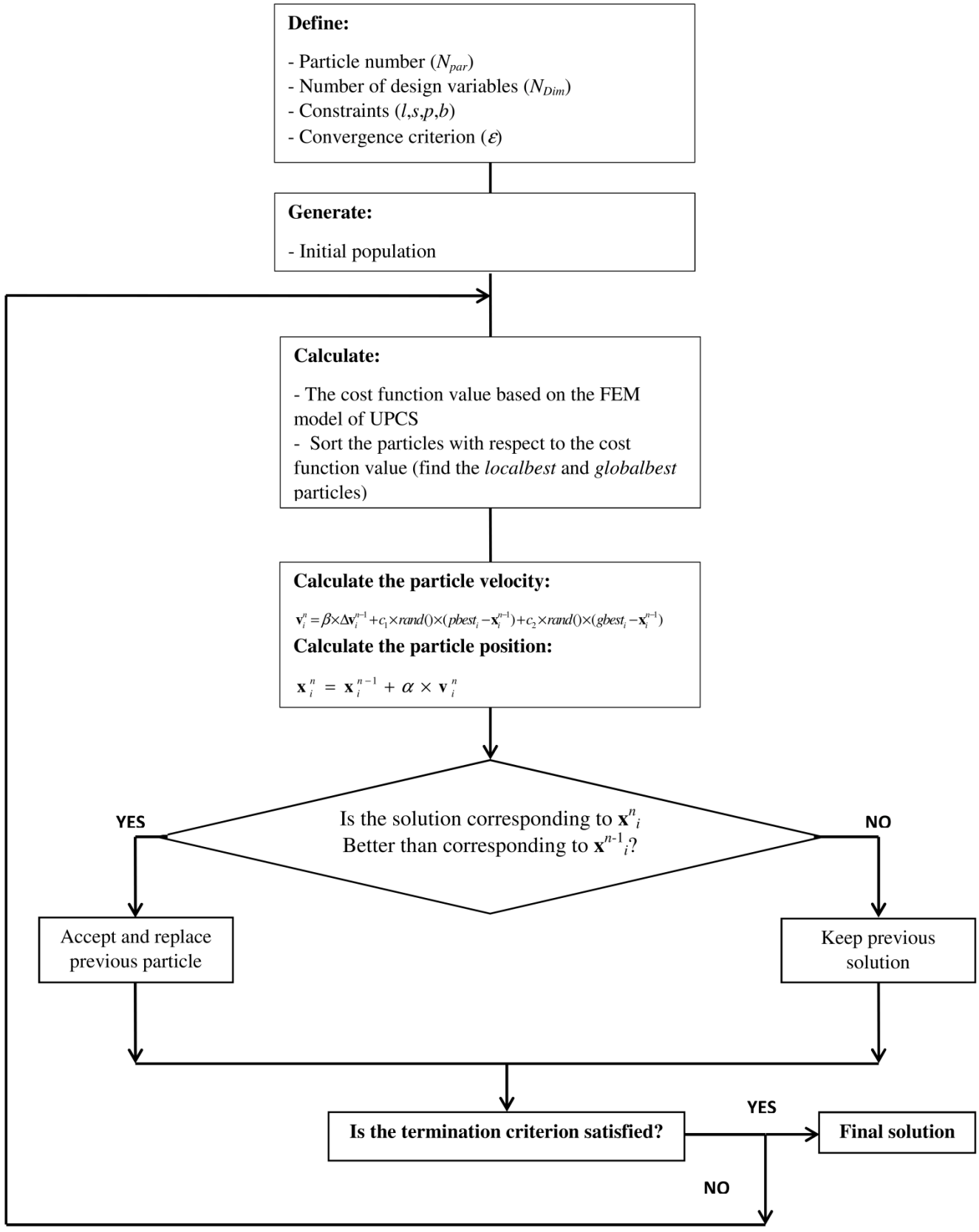

Fig. 8 The flowchart used for solving UPCS optimization problem

In this paper, the MATLAB is employed as a programming language for development of the code for optimizing of UPCS backfill layer cross-sectional area. The code consists of:

- FEM solver for heat conduction model in UPCS
- Momentum-type PSO solver for minimization of the cable bedding layer cross-sectional area.

7. Results and Discussion

The primary aim of underground power cable system design is to minimize the cable bedding cross-sectional area A_b. However, the maximum temperature of the cable conductor shall not exceed the best-found temperature of cable operation T_{opt}= 65˚C. In order to achieve these goals, the momentum-type PSO optimization is used. This section presents the application of the algorithm with the detailed analysis of results. The authors had performed a similar analysis as in papers [15], [55]. However, the new part is that the experimentally determined properties of thermal backfill (with an addition of Lafarge Gruntar^{TM} product) and comprehensive Campbell − de Vries model of soil thermal conductivity are included within the model of underground power cable system.

7.1. Response surface

Figures 9 and 10 show the maximum central cable (Fig. 6) conductor temperature $T_{c\ max}$ variations with the cable spacing *l* and different values of other design variables i.e. *s*, *p*, and *b*. Moreover, in Figs 9 and 10 the corresponding values of thermal bedding cross−sectional area A_b are presented. The conductor temperature is determined from the FEM model at the nodal location corresponding to the central cable gravity center.

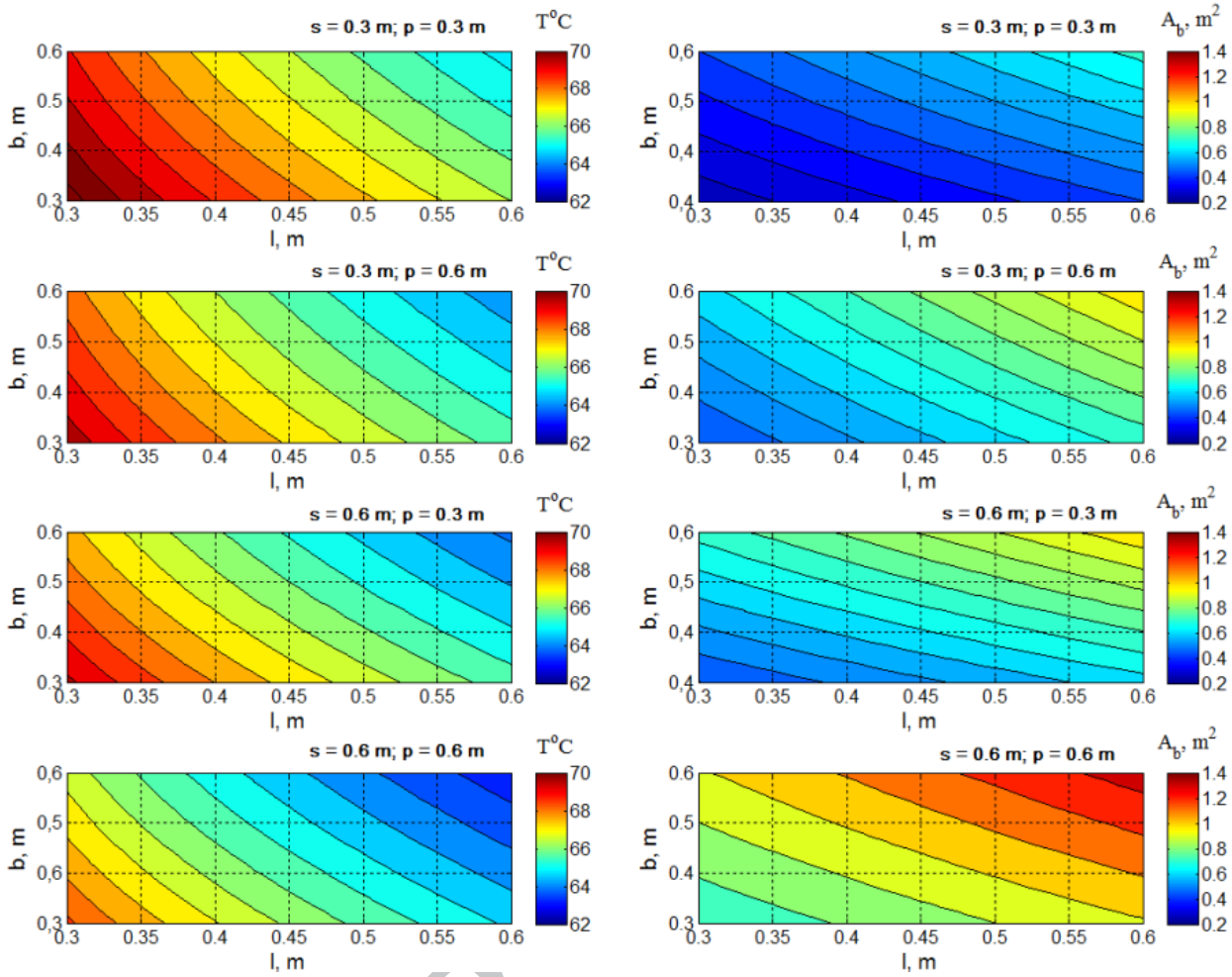

Fig. 9 The values of maximum conduction temperature and backfill area obtained for various values of *b* and *l* design variables and constant values of *s* and *p*.

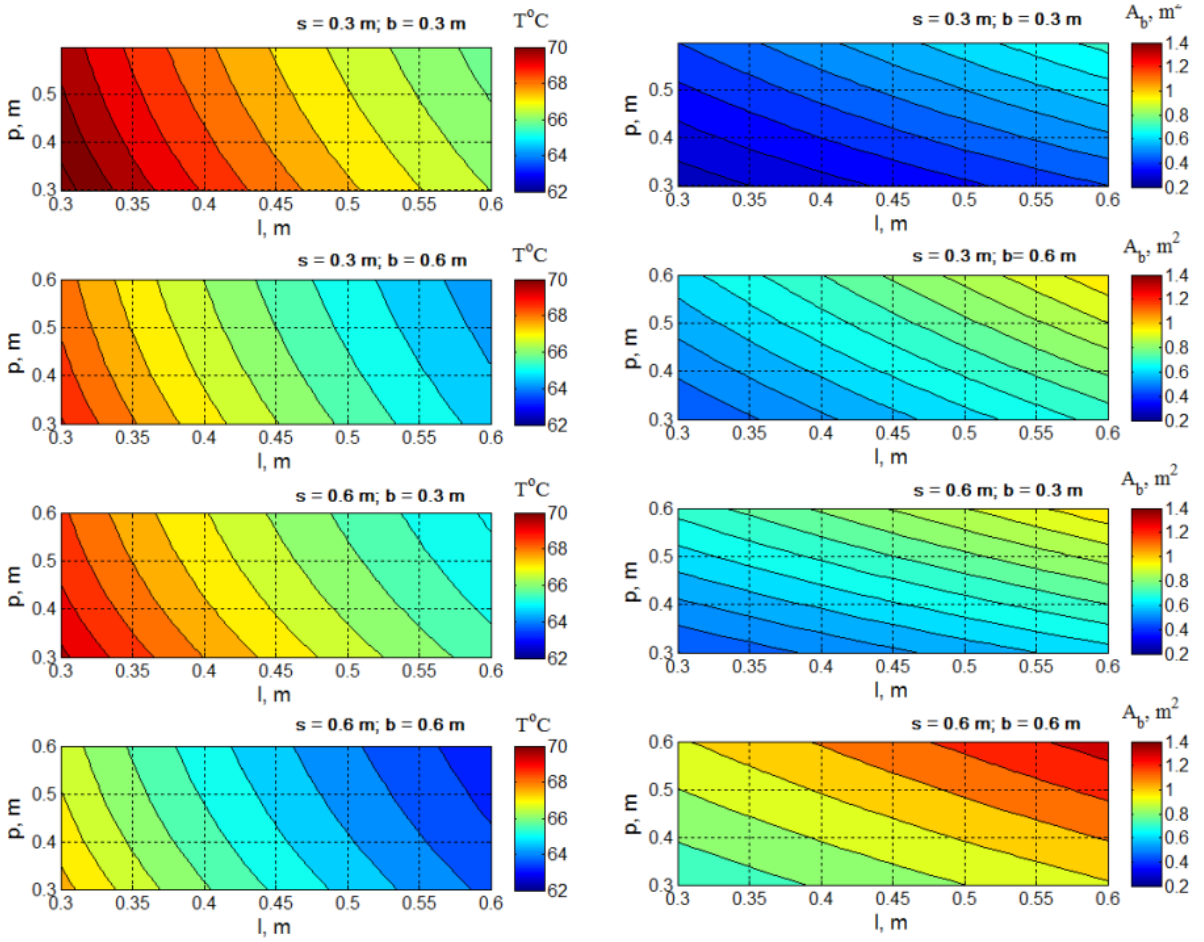

Fig. 10 The values of maximum conduction temperature and backfill area obtained for various values of *p* and *l* design variables and constant values of *s* and *b*.

In Figs 9 and 10 it can be seen that all values of the design variables strongly influence the temperature of the central cable conductor. The cable conductor temperature increases with the decrease in cable spacing *l*, and the decrease in *p*, *b* and *s* dimensions. On the other hand, the cable conductor temperature decreases with the increase of the cross−sectional area of thermal bedding layer. However, the larger the cross-sectional area, the greater the material and installation costs are. Thus, the optimization work has to be done to select the appropriate dimensions of thermal bedding layer.

7.2 Determination of thermal backfill cross-sectional dimensions

Figs. 9 and 10 reveal a strong influence of the design variables *b*, *p*, *s*, and *l* on the maximum cable conductor temperature. For economic reasons, the FTB bedding layer cross-sectional area shall be minimized while ensuring the conductor temperature close to T_{opt}= 65°C. Therefore, the momentum-type PSO algorithm (Eqs (21)−(26)) is applied to the global optimization problem, given by Eqs (28)-(30).

In order to analyze the momentum-type PSO algorithm behavior, 300 iterations are considered when presenting the computational results. The swarm sizes are assumed as N_{par} = 10, 20, and 30. Hence, the influence of swarm size on both the obtained global minimum of $F(\mathbf{x})$ function and the algorithm behavior can be studied.

The computations were performed for 5 runs and during each run best-found values of design variables varied no more than 0.01% for each size of the particle swarm. The detailed values of min, mean and max value of design variables for each run are given in Table 3.

Table 3 Summary of computational runs performed during the optimization of underground power cable system using momentum-type PSO.

				N_{par} = 10					
Run	F_{min}	F_{mean}	F_{max}	b_{min}	b_{mean}	b_{max}	p_{min}	p_{mean}	p_{max}
1	0.65509	26.8927	49.1943	0.59999	0.59999	0.6	0.2	0.2	0.2
2	0.65508	31.3347	46.3928	0.59999	0.6	0.6	0.2	0.2	0.2
3	0.6551	35.8579	49.8548	0.59999	0.59999	0.6	0.2	0.2	0.2
4	0.65508	33.2133	50.1879	0.59999	0.6	0.6	0.2	0.2	0.2
5	0.65509	35.4633	50.52	0.59999	0.59999	0.6	0.2	0.2	0.2
				N_{par} = 20					
1	0.65506	59.745	309.87	0.6	0.6	0.6	0.2	0.20028	0.20118
2	0.65507	25.0945	354.68	0.59999	0.6	0.6	0.2	0.20055	0.20208
3	0.65507	8.4	40.2795	0.6	0.6	0.6	0.2	0.20048	0.20236
4	0.65506	18.439	130.635	0.6	0.6	0.6	0.2	0.20046	0.20158
5	0.65506	11.737	81.67	0.6	0.6	0.6	0.2	0.20064	0.20276
				N_{par} = 30					
1	0.65502	14.42	77.156	0.59999	0.59999	0.6	0.20001	0.20002	0.20002
2	0.65502	11.038	44.979	0.59999	0.6	0.6	0.20001	0.20001	0.20002
3	0.65501	11.87	32.174	0.59999	0.59999	0.6	0.20001	0.20002	0.20002
4	0.65501	13.082	65.507	0.59999	0.6	0.6	0.20001	0.20002	0.20002
5	0.65502	10.481	50.872	0.59999	0.59999	0.6	0.2	0.20001	0.20002

				N_{par} = 10					
Run	s_{min}	s_{mean}	s_{max}	l_{min}	l_{mean}	l_{max}	T_{min}	T_{mean}	T_{max}
1	0.33288	0.33289	0.33289	0.59981	0.59999	0.6	65	65	65
2	0.33288	0.33289	0.33289	0.59981	0.6	0.6	65	65	65
3	0.33288	0.33289	0.33288	0.59981	0.59999	0.6	65	65	65
4	0.33288	0.33289	0.33289	0.59981	0.6	0.6	65	65	65
5	0.33288	0.33289	0.33289	0.59981	0.59999	0.6	65	65	65
				N_{par} = 20					
1	0.32546	0.33189	0.34379	0.59982	0.59999	0.6	65	65	65
2	0.32377	0.33233	0.34044	0.59997	0.6	0.6	65	65	65
3	0.33039	0.33241	0.33704	0.59999	0.6	0.6	65	65	65
4	0.32965	0.33195	0.33304	0.59993	0.6	0.6	65	65	65
5	0.32961	0.33202	0.33385	0.59997	0.6	0.6	65	65	65
				N_{par} = 30					
1	0.33252	0.33257	0.3326	0.59998	0.59999	0.6	65	65	65
2	0.33256	0.33258	0.3326	0.59997	0.59999	0.6	65	65	65
3	0.33256	0.33258	0.33266	0.59998	0.59999	0.6	65	65	65
4	0.33255	0.33258	0.3326	0.59998	0.59999	0.6	65	65	65
5	0.33254	0.33258	0.33267	0.59997	0.59999	0.6	65	65	65

The best found the solution of design variables (b, p, l, s), maximum central cable conductor temperature (T_{cmax}) and cross-sectional area of the cable bedding (A_b) are given in Table 4. The particle swarm sizes N_{par} = 10, 20, and 30 are considered during the computations.

Table 4 The best-found values of design variables (l,b,p,s), maximum temperature of cable conductor $T_{c\,\max}$, best-found values of cable bedding cross-sectional area A_b and a global minimum of cost function $F(\mathbf{x})$.

N_{par}	l, m	b, m	p, m	s, m	$T_{c\,\max}$, °C	A_b, m^2	$F(\mathbf{x})$
10	0.6	0.6	0.2	0.33288	65	0.65508	0.65508
20	0.6	0.6	0.2	0.33251	65	0.65506	0.65506
30	0.6	0.6	0.20002	0.32575	65	0.65501	0.65501

In the present computations, the application of momentum-type PSO solver ensured that the cable operates at the permitted temperature, and the cable bedding layer area is smaller than those obtained during the response surface tests. Therefore, the obtained results are satisfactory from the engineering point of view. However, some slight improvement may be made by combining different optimization solvers to reach an even better solution.

Fig. 11 presents the FEM model and temperature distribution obtained for the best-found values of design variables. For the best-found set of design variables (see Table 3, N_{par} = 30) the number of finite elements is E = 78851, and the number of nodes is of N = 39721. The grid independence studies were performed in a similar way to our previous work [33], and the maximum temperature of cable core do not vary more than 0.05ºC when increasing the node number with increasing node number. The triangular finite elements were applied for the discretization of heat conduction equation. The mesh was refined within the cable and thermal backfill domains to map the considerable temperature gradients correctly in those regions. An efficient method for assembly of finite element matrices [56] was employed in FEM solver [33]. The computational time for a single evaluation of cost function in PSO solver varied between 6 and 7 seconds (processor Intel Core i7 4700 mq, 8mb of RAM) depending on the FEM model created from the design variable set. The total time of computations varied from 5 hours (for N_{par} = 10) to 17.5 hours (for N_{par} = 30).

The advanced computational FEM model for liquid water and water vapor transport within the soil with buried power cable was presented by Kroener et al. [40]. The model includes Campbell −de Vries formula for soil thermal conductivity and allows to determine the transient variation of cable temperature and variation of water content within the soil. The model was verified experimentally, and the measured temperatures correspond well to the simulation results. The approach used in this paper is simplified since, from an engineering point of view, it is needed to perform the optimization within a short period of time. Since the cost function is evaluated from 3000 to 9000 times during the optimization, the model used in optimization shall be simplified, and explore the unfavorable condition for cable system design.

Due to the large size of heat transfer domain considered in this study, the closer view of FEM model is presented for the cable bedding area and the side cable laid in HDPE pipes. The temperature distribution is calculated for the entire UPCS including soil, thermal backfill, HDPE casing pipes and power cables. It can be seen that the maximum temperature of the central cable conductor is equal to 65°C.

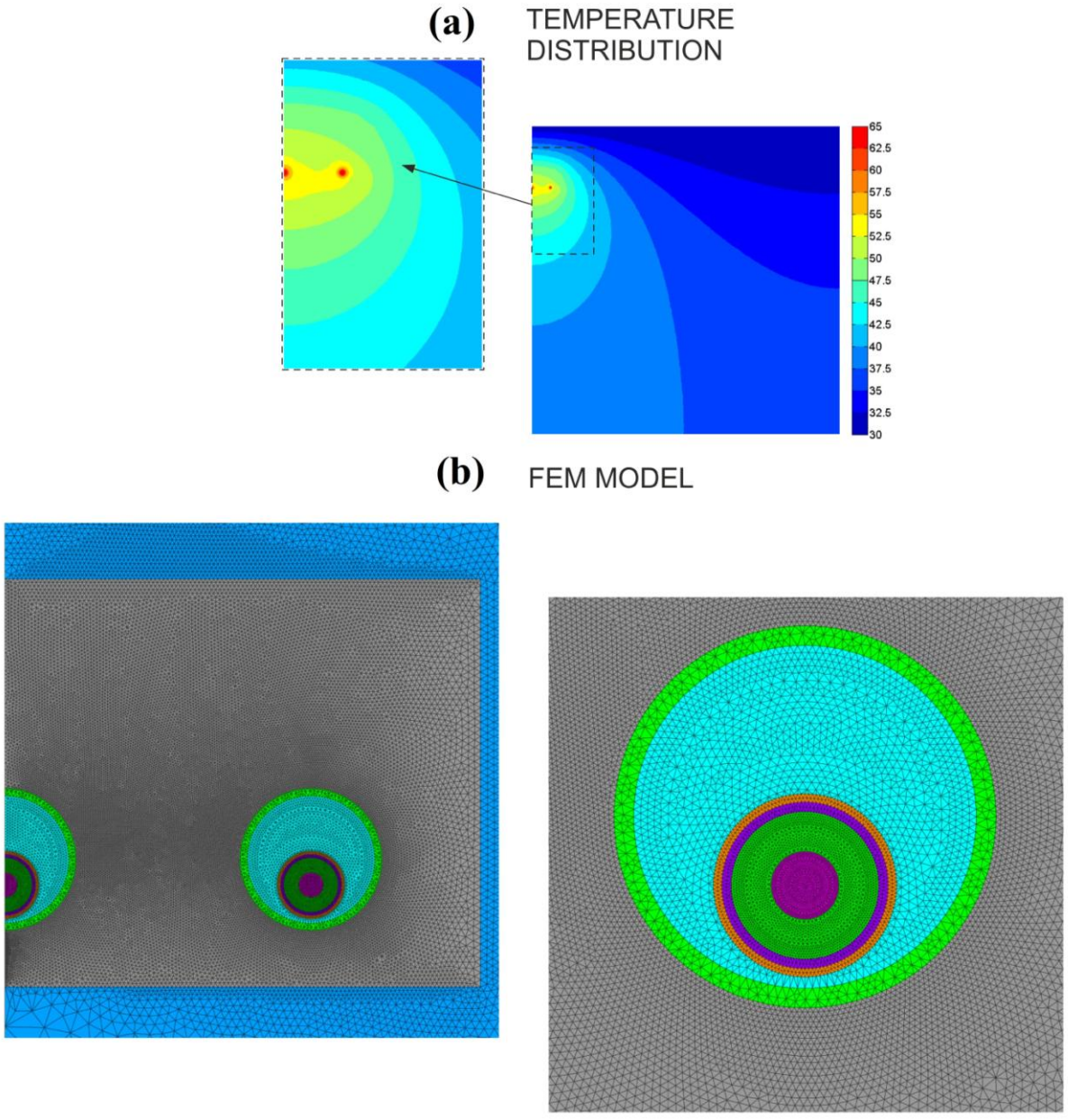

Fig. 11(a) Temperature distribution in a vicinity of cable bedding and the entire analyze UPCS (cable, bedding, mother ground), and (b) the FEM model created during the optimization procedure.

The heat is generated in the central and side cable conductors. The most favorable heat dissipation conditions occur for the side cable. Heat generated within the side cable core is conducted directly through the FTB layer to the mother ground on the cable right side. The unfavorable heat transfer conditions occur for the central cable where the generated heat is conducted through the FTB bedding and the side cables to the soil. Therefore, due to the cable temperature field interactions, the temperature of the central cable is the highest.

KD−2 PRO sensor ensures that the thermal conductivity measurements are valid with an accuracy of

± 10% for the soil thermal conductivity in a range of 0.2 to 6.0 W/(m K) which corresponds to λ_{soil} = 2.35 W/(m K). Thus, the reference value used in the computations i.e. λ_{soil} = 2.35 W/(m K) can be decreased or increased by 10%. The computations (with assumed N_{par} = 30) were also performed for λ_{soil} = 2.11 W/(m K) and 2.59 W/(m K). The obtained backfill area, for which the maximum cable core temperature is equal to 65°C are A_b = 0.87 m^2 for λ_{soil} = 2.11 W/(m K) and A_b = 0.61 m^2 for λ_{soil} = 2.59 W/(m K).

8. Concluding remarks

This paper presents an experimental determination of thermal conductivity for thermal backfill materials based on Gruntar^{TM} product. Gruntar^{TM} is an engineered developed mixture, which consists mainly of Portland cement, with other mineral additives as fly ash, gypsum, and limestone powder, among others. Gruntar^{TM} is characterized by a high degree of water absorption, high compaction, low shrinkage and suitably selected composition, which allows chemical binding of water. This paper reveals that the Gruntar^{TM} may also be applied as a component of thermal backfills that are used to protect cables from overheating. During the experimental investigation, the thermal backfills with the 5%, 10%, and 15% mass fraction of Gruntar^{TM} component are examined. The thermal conductivity of the proposed backfill material was determined as a function of water content. The thermal backfill with 15% of Gruntar^{TM} achieved the highest thermal conductivity of 1.02 W/(m K) in the dry state.

The primary function of cable backfills is to dissipate the heat efficiently away from the power cables and thus maintain cable temperature within the permissible limits. Newly developed cable backfill compositions provide better heat dissipation conditions, compared to the native soil. Thus, admissible cable systems ampacity may be raised around 10 to 15%. It may also result in a reduction of the cable conductor cross−sectional area, thereby considerably reducing investment costs. Another advantage of the suitable backfill material is the stability of its thermal conductivity in time. The constant thermal properties during the lifespan of the cable system provide its reliability in operation, thus eliminating the dry−zone effect (drying out of the soil or backfill around the cable, leading to the cable temperature increase) and allowable ampacity will be maintained for the entire lifetime of the underground cable system.

An electrical energy transmission line that consists of three underground power cables, placed in a flat (in−line) arrangement, is studied in this paper. To avoid the excessive mechanical loads the cables are situated in HDPE casing pipes filled with the sand−bentonite mixture (SBM). The HDPE casing pipes are buried directly in thermal backfill layer to protect the cables from overheating. Due to the substantial costs of backfill material (about 50 – 130$ per cubic meter), the cross-sectional area of bedding layer has to be minimized. The thermal properties of new cable backfill based on Gruntar^{TM} (with the mass fraction of 15 %) product is used in the case study. Also, the comprehensive Campbell − de Vries model of soil thermal conductivity was employed within a simulation model of the studied underground power cable

system. The Finite Element Method is used for determining the temperature distribution in underground power cable system while the momentum−type Particle Swarm Optimization (PSO) algorithm is applied to minimize the thermal backfill cross-sectional area.The application of momentum-type PSO algorithm has minimized the thermal backfill layer cross-sectional area while the applied dynamic penalty function has enabled not to exceed the optimal cable core temperature. Here the algorithm calculates the difference between the maximum and optimal temperatures of the cable core and tries to ensure that it is close to zero. In order to test the computational algorithm's behavior, the influence of algorithm parameters on solution convergence history is analyzed. For example, the influence of a number of particles on the value of obtained global minimum is studied. The particle number of 10, 20, and 30 is tested, and it is shown that for different particle numbers in the swarm, the particles reach the final solution that does not differ by more than 1%. In view of the results obtained in this study, the presented optimization method may be regarded as an efficient tool for optimizing the underground power cable systems.

Acknowledgements

The authors would like to acknowledge the ENERGOPROJEKT-KRAKÓW S.A. and LAFARGE POLAND for creative support during the numerical computations and material study of the underground power cables system presented in this study.

References

[1] Orton, H.: History of underground power cables. Electrical Insulation Magazine, IEEE **29**(4), 52–57 (2013).

[2] Morishita, Y.: Technical trends of high voltage and large capacity underground power cables. IEEJ Transactions on Electrical and Electronic Engineering **2**(5), 531–535 (2007).

[3] Metwally, I., Al-Badi, A., Al Farsi, A.: Factors influencing ampacity and temperature of underground power cables. Electrical Engineering **95**(4), 383–392 (2013).

[4] Dai, D., Zhang, X., Wang, J.: Calculation of AC resistance for stranded single-core power cable conductors. Magnetics, IEEE Transactions on **50**(11), 1–4 (2014).

[5] ENERGETIK DK: Cable action plan 132 - 150 kV grids (2009).

[6] Del Valle, Y., Venayagamoorthy, G.K., Mohagheghi, S., Hernandez, J.C., Harley, R.G.: Particle swarm optimization: basic concepts, variants and applications in power systems. Evolutionary Computation, IEEE Transactions on **12**(2), 171–195 (2008).

[7] Kovač, N., Sarajčev, I., Poljak, D.: A numerical–stochastic technique for underground cable system design. IEE Proceedings-Generation, Transmission and Distribution **153**(2), 181–186 (2006).

[8] Al-Saud, M., El-Kady, M., Findlay, R.: A novel finite-element optimization algorithm with applications to power cable thermal circuit design. In: Power Engineering Society General

Meeting, 2007. IEEE, pp. 1–8. IEEE (2007).

[9] Moutassem, W., Anders, G.J.: Configuration optimization of underground cables for best ampacity. Power Delivery, IEEE Transactions on **25**(4), 2037–2045 (2010).

[10] [Zarchi, D.A., Vahidi, B., Haji, M.M.: Optimal configuration of underground cables to maximise total ampacity considering current harmonics. Generation, Transmission & Distribution, IET **8**(6), 1090–1097 (2014).

[11] del Pino-López, J.C., Cruz-Romero, P., Serrano-Iribarnegaray, L., Martínez-Román, J.: Magnetic field shielding optimization in underground power cable duct banks. Electric Power Systems Research **114**, 21–27 (2014).

[12] Campbell, G., Jungbauer Jr, J., Bidlake, W., Hungerford, R.: Predicting the effect of temperature on soil thermal conductivity. Soil Science **158**(5), 307–313 (1994).

[13] TELE-FONIKA Company: High voltage cables. 1st ed. Cracow (in Polish) (2012).

[14] Cisek, P., Ocłoń, P., Pilarczyk, M.: Thermal analysis of operating conditions for the 400 kV underground power cable transmission line as a power plant delivery system. Rynek Energii114, 70–77 (in polish) (2014).

[15] Ocłoń, P., Cisek, P., Taler, D., Pilarczyk, M., Szwarc, T.: Optimizing of the underground power cable bedding using momentum-type particle swarm optimization method. Energy 92 (2015), 230-239.

[16] Electric Power Research Institute Inc.: Increased Power Flow Guidebook - Underground Cables, Final Report (December 2003).

[17] Lafarge: Press Communication on Gruntar, online version. (2012), www.lafarge.pl (in Polish)

[18] Decagon Devices Inc.: KD2 Pro Thermal Properties Analyzer. (2014).

[19] Righini F., Bussolino G. C., Rosso A., Roberts R. B., Thermal conductivity by a pulse-heating method: Theory and experimental apparatus, International Journal of Thermophysics, 11 (1990), pp 629-641.

[20] Campbell G.S., Calissendorff C., Williams J.H., Probe for measuring soil specific heat using a heat-pulse method, Soil Science Society of America Journal 55 (1) (1991), pp.291-293.

[21] Bristow K.L., Campbell G.S., Calissendorff K., Test of a heat-pulse probe for measuring changes in soil water content, Soil Science Society of America Journal 57 (4) (1993) pp. 930-934.

[22] American Society for Testing and Materials (ASTM) standard E1582 – 14, Standard Practice for Calibration of Temperature Scale for Thermogravimetry.

[23] IEC 60287-2-1: Electric Cables - Calculation of the current rating - Part 2: Thermal resistance - Section 1: Calculation of the thermal resistance (1995).

[24] Sepaskhah, A. R., Boersma, L.: 1979, *Thermal conductivity of soils as a function of temperature and water content*, Soil Sci. Soc. Am. J. 43, 439–444.

[25] McInnes, K.: 1981, *Thermal conductivities of soils from dryland wheat regions in Easter*

Washington. MSc thesis, Washington State University.

[26] Tarnawski V. R., Leong W. H., Thermal Conductivity of Soils at Very Low Moisture Content and Moderate Temperatures, Transport in Porous Media 41 (2000), pp.137–147.

[27] Tien, Y.m., Chu, C.A., Wu, P.L., Chuang, W.S., Chung, Y.J.: Improved measurement and a predictive model for thermal conductivity of sand-bentonite mixtures. Journal of GeoEngineering **5**(2), 51–60 (2010).

[28] de Lieto Vollaro, R., Fontana, L., Vallati, A., Experimental study of thermal field deriving from an underground electrical power cable buried in non-homogeneous soils. Applied Thermal EngineeringVolume 62, Issue 2, 2014, Pages 390-397.

[29] De Lieto Vollaro, R., Vallati, A., Study of a model for the evaluation of the heat losses from electric cables buried according to the norm standard. Advanced Materials ResearchVolume 650, 2013, Pages 437-442.

[30] De Lieto Vollaro, R., Fontana, L., Quintino, A., Vallati, A.Improving evaluation of the heat losses from arrays of pipes or electric cables buried in homogeneous soil. Applied Thermal Engineering Volume 31, Issue 17-18, December 2011, Pages 3768-3773.

[31] Galli, G., Vallati, A.Equilibrium heat and moisture transfer in soils with heat sources. International Journal of Heat and Technology Volume 29, Issue 1, 2011, Pages 33-38.

[32] De Lieto Vollaro, R., Fontana, L., Vallati, A.Thermal analysis of underground electrical power cables buried in non-homogeneous soils. Applied Thermal EngineeringVolume 31, Issue 5, April 2011, Pages 772-778.

[33] Ocłoń, P., Cisek, P., Pilarczyk, M., D., Taler: Numerical simulation of heat dissipation processes in underground power cable system situated in thermal backfill and buried in a multilayered soil. En Conv Men 95, 352-370 (2015).

[34] Karahan M., Kalenderli Ö., *Coupled Electrical and Thermal Analysis of Power Cables Using Finite Element Method*, Heat Transfer - Engineering Applications, Prof. Vyacheslav Vikhrenko (Ed.), ISBN:978-953-307-361-3, InTech (2011).

[35] Hiivala, L.J., Landinger, C.C., Conductors. chapter in Electrical Power Cable Engineering, Third Edition, CRC Press (2014).

[36] IEC 287: Calculation of the continuous current rating of cables (100%) load factor, IEC Publication 287 (1982).

[37] Salata, F., Nardecchia, F., de Lieto Vollaro, A., Gugliermetti, F.: Underground electric cables a correct evaluation of the soil thermal resistance. Applied Thermal Engineering **78** (0), 268 – 277 (2015).

[38] Al-Saud, M., El-Kady, M., Findlay, R.: A new approach to underground cable performance assessment. Electric Power Systems Research **78**(5), 907–918 (2008).

[39] Hwang, C.C., Jiang, Y.H.: Extensions to the finite element method for thermal analysis of

underground cable systems. Electric Power Systems Research **64**(2), 159–164 (2003).

[40] Kroener, E., Vallati, A., Bittelli, M.: Numerical simulation of coupled heat, liquid water and water vapor in soils for heat dissipation of underground electrical power cables. Applied Thermal Engineering **70**(1), 510–523 (2014).

[41] Papagiannopoulos, I., Chatziathanasiou, V., Exizidis, L., Andreou, G., De Mey, G., Wiecek, B.: Behaviour of the thermal impedance of buried power cables. International Journal of Electrical Power & Energy Systems **44**(1), 383–387 (2013).

[42] Bittelli, M., Ventura, F., Campbell, G. S., Snyder, R. L., Gallegati, F., Pisa, P. R.: Coupling of heat, water vapor, and liquid water fluxes to compute evaporation in bare soils. Journal of Hydrology **362**, 191–205 (2008).

[43] Bittelli M., Campbell G.S., Tomei F., *Soil Physics with Python. Transport in the Soil–Plant–Atmosphere System*, Oxford University Press (2015).

[44] de Vries, D.A.: Thermal properties of soils. Physics of plant environment (1963).

[45] Peters-Lidard C. D., Blackburn E., Liang X., Wood E. F., *The Effect of Soil Thermal Conductivity Parameterization on Surface Energy Fluxes and Temperatures*, Journal Of The Atmospheric Sciences 55 (1998), pp. 1209-1224.

[46] Lu S., Ren T., Gong Y., Horton R., *An Improved Model for Predicting Soil Thermal Conductivity from Water Content at Room Temperature*, Soil Sci. Soc. Am. J. 71 (2007), pp. 8-14.

[47] Campana, E.F., Fasano, G., Pinto, A.: Dynamic analysis for the selection of parameters and initial population, in particle swarm optimization. Journal of Global Optimization, 48:347-397 (2010).

[48] Beheshti, Z., Shamsuddin, S.M., Yuhaniz, S.S.: Binary Accelerated Particle Swarm Algorithm (BAPSA) for discrete optimization problems. Journal of Global Optimization, 57:549-573 (2013).

[49] Kaucic, M.: A multi-start opposition-based particle swarm optimization algorithm with adaptive velocity for bound constrained global optimization. Journal of Global Optimization, 55:165-188 (2013).

[50] Liu, J.L., Lin, J.H.: Evolutionary computation of unconstrained and constrained problems using a novel momentum-type particle swarm optimization. Engineering Optimization **39**(3), 287–305 (2007).

[51] Kennedy, J., Eberhart, R.C.: Particle swarm optimization. In: Proceedings of IEEE International Conference on Neural Networks, vol. 4, pp. 1942–1948 (1995).

[52] Kennedy, J., Eberhart, R.C., Shi, Y.: Swarm intelligence. Morgan Kaufmann (2001).

[53] Trelea, I.C.: The particle swarm optimization algorithm: convergence analysis and parameter selection. Information processing letters **85**(6), 317–325 (2003).

[54] Popiel, C.O., Wojtkowiak, J., Biernacka, B.: Measurements of temperature distribution in ground. Experimental thermal and fluid science **25**(5), 301–309 (2001).

[55] Ocłoń P., Taler D., Cisek P., Pilarczyk M., FEM-Based Thermal Analysis of Underground Power

Cables Located in Backfills Made of Different Materials, Strength of Materials, Vol. 47, No. 5 (2015), 770-780.

[56] Cuvelier F, Japhet C, Sarella G. An efficient way to perform the assembly of finite element matrices in Matlab and Octave. Technical Report. 8305, Universit´e Paris 13; 2013.

[57] Online resource: ground temperature data (provided by Potsdam Institute for Climate Impact Research):https://www.pik-potsdam.de/services/climate-weather-potsdam/climate-diagrams/ground-temperature.

Highlights:

- New thermal backfill composition is proposed and tested.
- Backfill thermal conductivity as a function of water content is presented.
- The laboratory test stand as well as experimental data are discussed.
- Campbell – de Vries model is adopted in the thermal conductivity computations.
- The design optimization of UPCS is presented in detail.